Experiments and simulations of an industrial assembly with different types of nonlinear joints subjected to harmonic vibrations

T Roncen, Jean-Jacques Sinou, J-P Lambelin

T. Roncen, J-J. Sinou and J-P. Lambelin, Experiments and simulations of an industrial assembly with different types of nonlinear joints subjected to harmonic vibrations, Journal of Sound and Vibration, 458, 458-478, 2019.
doi.org/10.1016/j.jsv.2019.06.029

Experiments and simulations of an industrial assembly with different types of nonlinear joints subjected to harmonic vibrations

T. Roncen[a,b], J-J. Sinou[b,c] and J-P. Lambelin[a]
[a] *CEA, DAM, CESTA, F-33114 Le Barp, France*
[b] *Laboratoire de Tribologie et Dynamique des Systèmes UMR CNRS 5513, Ecole Centrale de Lyon, France.*
[c] *Institut Universitaire de France, 75005 Paris, France.*

Abstract

The structure Harmony-Gamma is a metallic assembly representative of an industrial structure for which the vibratory response is influenced by the apparition of nonlinear phenomena within two specific types of joints, the first corresponding to friction joints and the second to elastomer joints. Firstly, the paper presents the experimental procedure and results obtained for this structure. Secondly, a global methodology for modeling and simulation of the nonlinear vibrational response is set up.

The experiments are performed for longitudinal and transverse swept sine experiments. First of all, swept sine experiments are performed at low excitation levels on the structure in order to update a linear finite-element model. Then, the evolution of the frequency response function is studied at increasing excitation levels in order to identify the contribution of the nonlinear effects on the global vibrational response of the system.

The methodology for modeling and simulation consists of five steps. Firstly, a finite-element model of the structure is presented and updated in order to be representative of the structure when it is excited at low excitation levels. This model is then reduced using a hybrid sub-structuring technique. Thirdly, the nonlinear models of the friction and elastomer joints are added. The resulting optimization problem is solved by means of the Harmonic Balance Method (HBM) coupled with a Newton-Raphson continuation and a condensation process. Lastly, the simulation results are compared to the experimental results in order to validate the development of the finite element model for the nonlinear industrial structure Harmony-Gamma with nonlinear joints of different natures and to achieve a refined understanding of the nonlinear phenomena and their origin.

1. Introduction

The vibrational response of mechanical systems used to be mainly studied by means of a linear analysis. Indeed, numerical simulations for both the modal analysis and frequency response function of linear systems are implemented in every finite-element software package, and are widely used in industry. However, the experimental vibration study of industrial assemblies often shows a strong dependency of the response on the excitation level, which cannot be taken into account with linear simulations. The nonlinearities causing these disruptions may exhibit various origins: large displacements, contact, friction in the joints, or non-elastic compounds. The consequences of such nonlinearities are a dependency of eigenfrequencies and dissipation on the input amplitude, discontinuities in the frequency response and a multi-harmonic response to a mono-harmonic excitation. In the present study, two nonlinearities are at stake: friction of contact blades and the non-elastic behavior of elastomer materials in rubber isolators. These two nonlinearities have a double effect on the assembly. The friction conveys the relaxation of a constraint in a joint by the apparition of sliding, while the elastic and dissipative properties of the elastomer mainly depend on its deformation amplitude. Even though the nonlinearities are localized on the structure, they have a global impact on the softening and the damping of the structure.

Therefore, the incorporation of nonlinear joints into complex mechanical structures raises new challenges. An efficient modeling of these nonlinearities as well as their inclusion in finite element models is crucial for studying and analysing the nonlinear dynamic behavior of such mechanical systems. The resulting complexity increase of the nonlinear differential equations requires new simulation tools to solve the equations in a time-efficient way. In this regard, various nonlinear computational techniques have been proposed over the years. Among them, the Harmonic Balance Method (HBM) is one of the most popular for approximating the

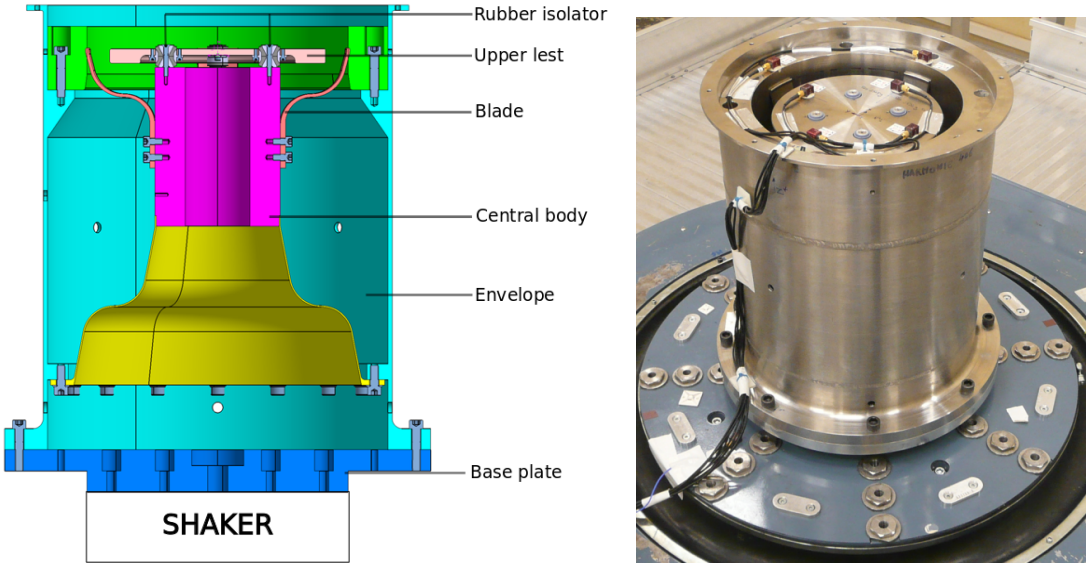

(a) (b)

Figure 1: The structure Harmony-Gamma (a) cross-section view and (b) photography

stationary nonlinear responses of mechanical systems [1]. It has been used in various nonlinear applications involving dry frictions [2, 3] or rotatory machines [4]. A numerical application has also been proposed in the work of Jaumouillé et al. [5] with rubber isolators. More recently, Claeys et al. [6, 7] presented an application of nonlinear simulations using the HBM on an industrial finite element model with contact blades.

Nowadays, experiments and simulations on nonlinear mechanical systems are often conducted alongside. The comparison between the experimental tests and the results of the numerical simulations provide, on the one hand a validation of the modeling and the simulation and, on the other hand, a better understanding of the experimental results and the physical contributions on the nonlinear behaviors. Having good confidence in the modeling and simulations is nowadays a crucial point and one of the primary objectives in industry. This allows to minimize the need for conducting many expensive experimental tests for the design of complex industrial systems. To be able to conduct such confrontations between experimental tests and numerical simulation for nonlinear mechanical systems is highly recommended and relevant but also more difficult due to the presence of nonlinearities. However, to conduct such an analysis is now essential to optimize the behavior of mechanical systems in regard to their non-linear dynamic behavior.

In the present study, the nonlinear behavior of a complex structure, named Harmony-Gamma, is investigated. This structure includes both nonlinear frictional and elastomer elements. Simulations with nonlinearities of different natures have never been compared to experimental results for industrial structures. So the main challenge of this paper is to study this type of problem. A secondary objective and a major contribution of this study is the use of simulations to get a better insight into the nonlinear phenomena at stake.

This paper is divided into three parts. Firstly, a brief description of the Harmony-Gamma test structure and the analysis of various experimental data from vibrational tests on a bench in the CEA laboratory are presented. Secondly, a finite-element model is developed (linear elements, reduction method, friction and elastomer modeling) and updated for the different experimental settings. The nonlinear simulation method, namely the Harmonic Balance Method, is then presented alongside a condensation process dedicated to the introduction of friction and elastomer joints in a linear reduced finite-element modeling. Finally, results from the nonlinear numerical simulations are compared to the experimental results, and performed with various options of activation / deactivation of the nonlinearities. This last part is one of the parts that comprise the originality of the study, which proposes to use numerical simulations in order to achieve a better understanding of the dynamical response of structures governed by coupled nonlinearities of different natures.

2. Presentation of the structure Harmony-Gamma

The Harmony-Gamma structure is represented in Figure 1 with a cross-section view (left) and a photograph of the assembly mounted on the shaker. The structure is composed of three main parts: a central

Component	Material	Dimensions (mm) Maximum / Height	Mass (kg)
Central body	Stainless steel 304L	160 / 300	11.92
External envelope	Stainless steel 304L	204 / 420	44.88
Blade (x4)	High resistance steel Z8-cnd17-04	65 / 118	0.1086
Base plate	Aluminum 2017A	204 / 40	9.47
Upper body	Stainless steel 304L	206.5 / 13.5	2.49

Table 1: Properties of the components of the assembly

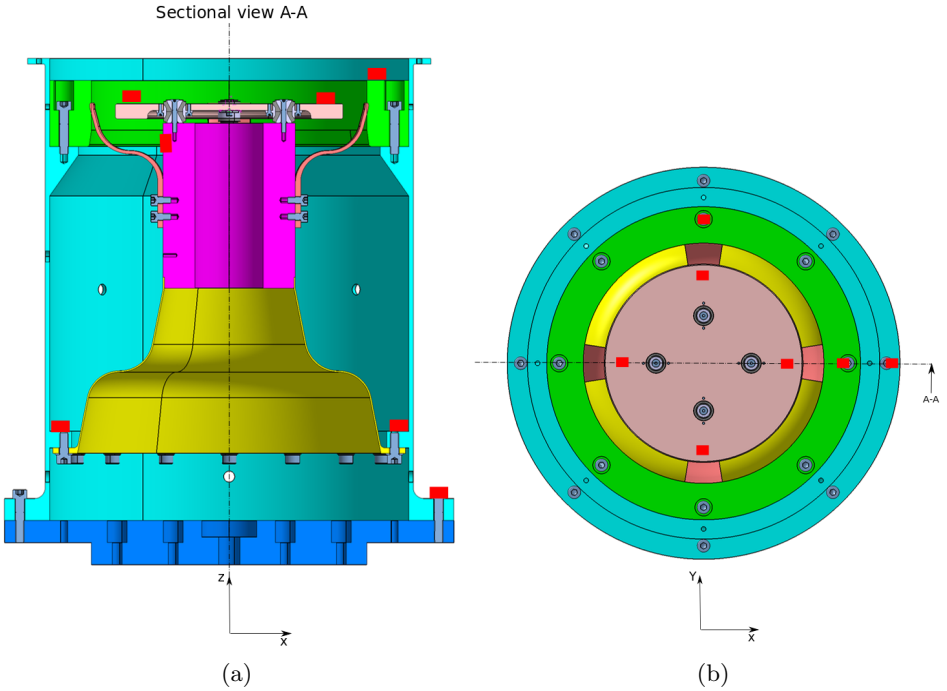

(a) (b)

Figure 2: Positioning of the accelerometers (red) (a) cross section (b) top view

body, an upper body and an external envelope. During the assembly, the central body is inserted inside the envelope from the bottom. The four blades are compressed in such a way that contact is always kept, even during vibration experiments. At this stage, the structure is identical to Harmony, which was studied previously in [6, 7]. To obtain the structure Harmony-Gamma, an upper ballast named "'upper body"' is added to the central body by means of four identical rubber isolators. These rubber isolators will favor the softening effect for the dynamic behavior of the whole structure and an increase in energy dissipation, while the friction blades will be responsible for the friction at high excitation levels. The assembly is presented in Figure 1 with a base plate that couples the assembly to the shaker. The different properties of the assembly are detailed in Table 1. The masses were measured experimentally. The structure Harmony-Gamma is instrumented with 11 tri-axial accelerometers that are represented in Figure 2. The instrumentation is identical for longitudinal and transverse swept sine experimental tests.

3. Measurement of the vibratory response

3.1. Longitudinal excitation

An industrial shaker of maximal force 27 kN is used to excite the structure vertically. The structure is bolted onto a base plate that is itself bolted onto the mobile part of the shaker. Under vertical excitation, an anti-resonance will appear during the experiments at the base plate, around the first resonance mode. The acceleration will always be null at the frequency of the anti-resonance on the base plate, so it is not possible to control the input in acceleration on any point of the base plate. Hence, a control in current intensity delivered by the shaker is used instead. This condition is close to control in force, because of the linear relationship between force and intensity delivered by the shaker. Actually, this linear relation is only an approximation of reality, and nonlinear effects linked to the frequency or the excitation level may

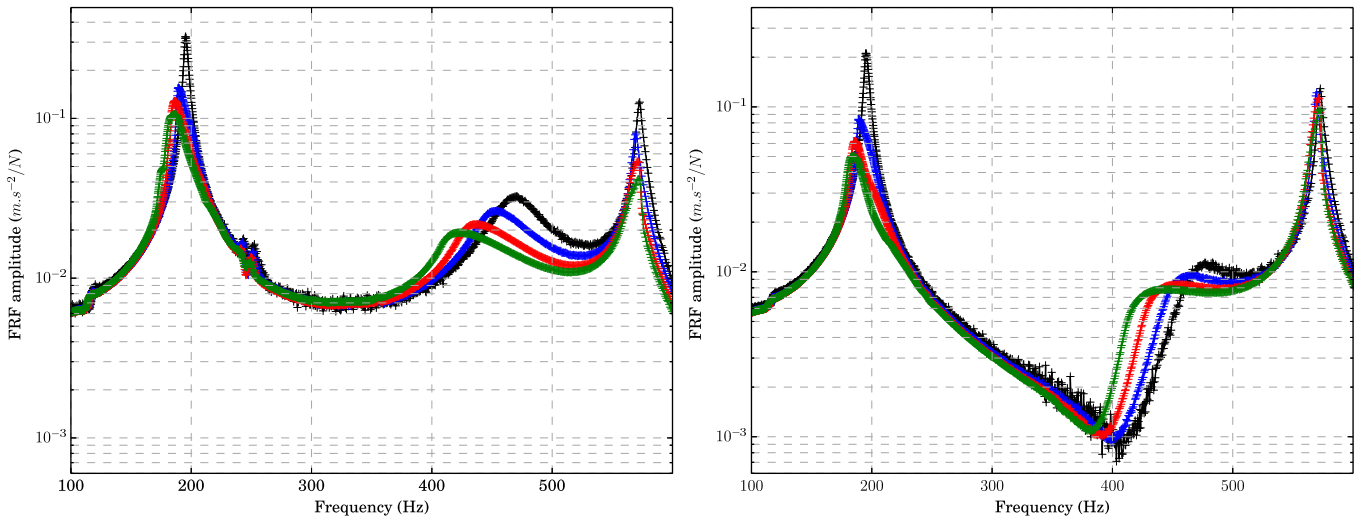

Figure 3: Experimental longitudinal FRFs obtained for the accelometers on (a) the upper body and (b) the central body for harmonic input excitations of 162 N (black), 813 N (blue), 1625 N (red) and 9748 N (green)

appear. The relation between force and intensity for the shaker has not been characterized. Therefore, in the following study, a linear relationship between the force and the intensity is assumed, unless mentioned otherwise. To calculate the force, the acceleration is measured at low frequencies for a given intensity input. The delivered force is then equal to the product of the acceleration by the mobile mass of the shaker added to the mass of the whole structure.

With the experimental configuration presented in Figure 1, the Harmony-Gamma structure is subjected to longitudinal harmonic excitations, with a frequency slowly varying over time (swept-sine experiments). Firstly, the experimental eigenfrequencies of the structure are identified for a low excitation level swept sine experiment (a low intensity delivered by the shaker). The first, second and third resonance frequencies are at 196 Hz, 478 Hz and 576 Hz, respectively. The frequency response functions (FRFs) are defined as the measured acceleration response divided by the force input. The experimental FRF are plotted for different excitation levels and for two accelerometers in Figure 3a (accelerometer positioned on the upper body) and on Figure 3b (accelerometer positioned on the central body).

Due to the existence of nonlinearities of distinct natures (local stick-slip behavior for the contact blades and elastomer properties for rubber isolators), the experimental dissociation of the nonlinear active phenomena is a difficult task. *A priori*, one cannot understand which nonlinearity is responsible for which shift in frequency or increase in energy dissipation. In this section only observations on the evolution of the response of the structure by increasing excitation levels are proposed. The numerical simulations presented further in this work will allow some insight into the role of the nonlinearities in the global response of the structure and the potential shift in frequency peaks with increasing excitations level. Considering experiments performed for excitation levels, the following basic observations can be made. the first peak is slightly shifted towards lower frequencies with a flattening effect when the excitation level increases, reflecting a nonlinear softening and an increase of dissipation. the second resonance mode is also affected by the nonlinearities, with a softening effect and an increase in dissipation (as seen for the first mode), but without any visible flattening effect. the third mode seems to have a rather constant resonance frequency, and a peak maximum that decreases as the excitation level increases. These effects of softening or increase in dissipation are visible on all of the accelerometers of the structure. Therefore, even though the friction and elastomer joints are localized, they induce a significant effect on the global response of the structure and give the latter a non-negligible nonlinear vibrational behavior. Consequently, it is crucial to take into account these nonlinearities in the design of such complex structures.

For the reader information, a preliminary settling has been performed before the first set of tests in order to avoid a wrong conclusion due to an initial uncontrolled evolution of the structure behavior. Indeed an initial variability of the frequency modes during the preliminary settling was observed due to a strong dependence on the clamping of the base plate to the shaker as well as a initial running-in period of the joints at the interface between the base plate and the shaker. After these first settling running tests, the

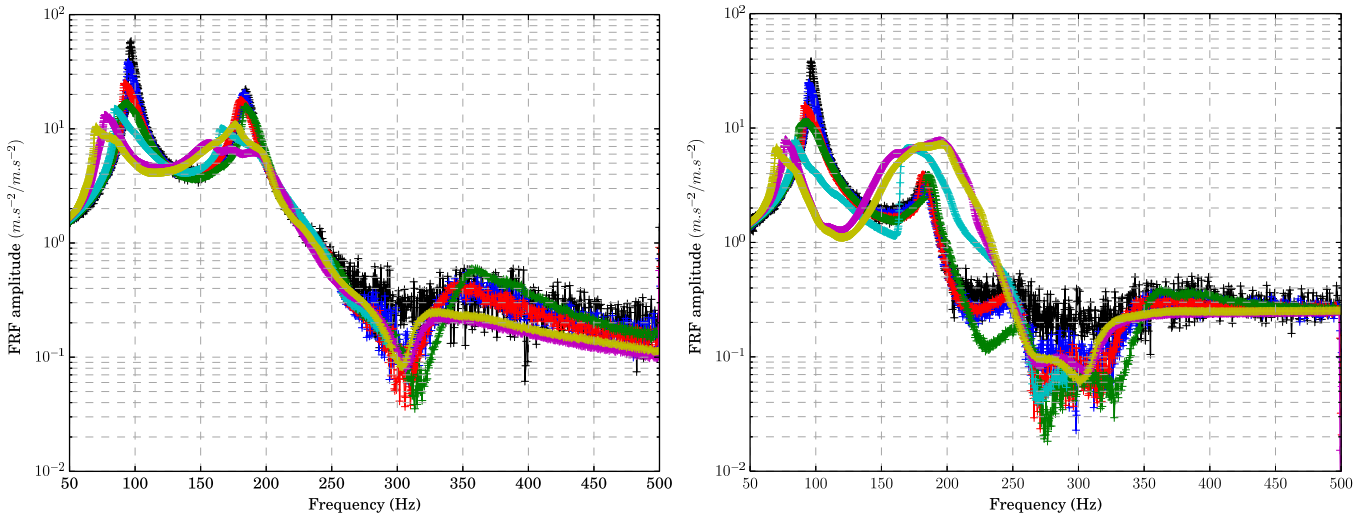

Figure 4: Experimental transverse FRFs obtained on the accelerometers positioned on (a) the upper body and (b) the central body for swept-sine experiments of excitation levels: 0.2 m s^{-2} (black), 0.5 m s^{-2} (blue), 1 m s^{-2} (red), 3 m s^{-2} (green), 5 m s^{-2} (cyan), 10 m s^{-2} (magenta) an 15 m s^{-2} (yellow)

repeatability of experimental tests has been successfully verified. The only slight shift in frequency can be associated with the second resonance mode. It is shown later in this work that the second mode is mainly related to the rubber isolators, so the variability is linked to two physical phenomena: the Mullins effect and the potential elevation of the room temperature.

3.2. Transverse excitation

The Harmony-Gamma structure has also been studied under transverse excitation. The friction blades and the rubber isolators are then loaded differently. The experimental setting that allows transverse excitation on the structure Harmony-Gamma slightly differs from the longitudinal setting, with the adding of an extra table between the base plate and the shaker. The shaker is controlled in order to impose a constant acceleration amplitude on a control accelerometer positioned on the base plate. Indeed, the problem of the anti-resonance observed for longitudinal excitations (see Section 3.1) does not exist for transverse excitations. The excitation levels are thus defined as base accelerations. The FRF is then defined as the ratio between the output acceleration and the input acceleration at the base plate, which does not require any calculation step.

First, the linear resonance modes of the structure have been identified with a transverse swept sine experiment in the frequency bandwidth [50;500] Hz. The main resonance peaks are observed at 95 Hz, 184 Hz and 354 Hz, and the modal experimental identification also indicates the presence of a tilting mode at 256 Hz. Then an increase in the excitation level is performed as follows: 0.2 m s^{-2}, 0.5 m s^{-2}, 1 m s^{-2}, 3 m s^{-2}, 5 m s^{-2}, 7 m s^{-2}, 10 m s^{-2} and 15 m s^{-2}. The FRFs are obtained at the top of the upper body and of the central body, and are represented in Figure 4a and Figure 4b, respectively. Similarly to what was observed for the longitudinal experiments, nonlinear phenomena in the global response of the structure are detected. The first resonance frequency decreases with the acceleration input, while the modal damping is increased. The second mode is initially at 184 Hz and has complex behavior. First, an increase in the dissipation and a softening of the resonance mode with the increase of the excitation level are observed. In the frequency range [150;200] Hz, an amplitude saturation with several bumps appears and becomes larger as the excitation level increases. Then, at the highest level of excitation, the resonance peak may reappear distinctly around 180 Hz (see Figure 4a). These experimental results on the second resonance mode highlight the contribution of the nonlinear joints to the global response of the structure. Furthermore, the experimental observations are quite complex to understand, because of the potential coupling between the nonlinearities of different nature (friction blades and rubber isolators) for a given frequency. As previously explained, all the experimental tests are performed by having taken care beforehand to perform a settling.

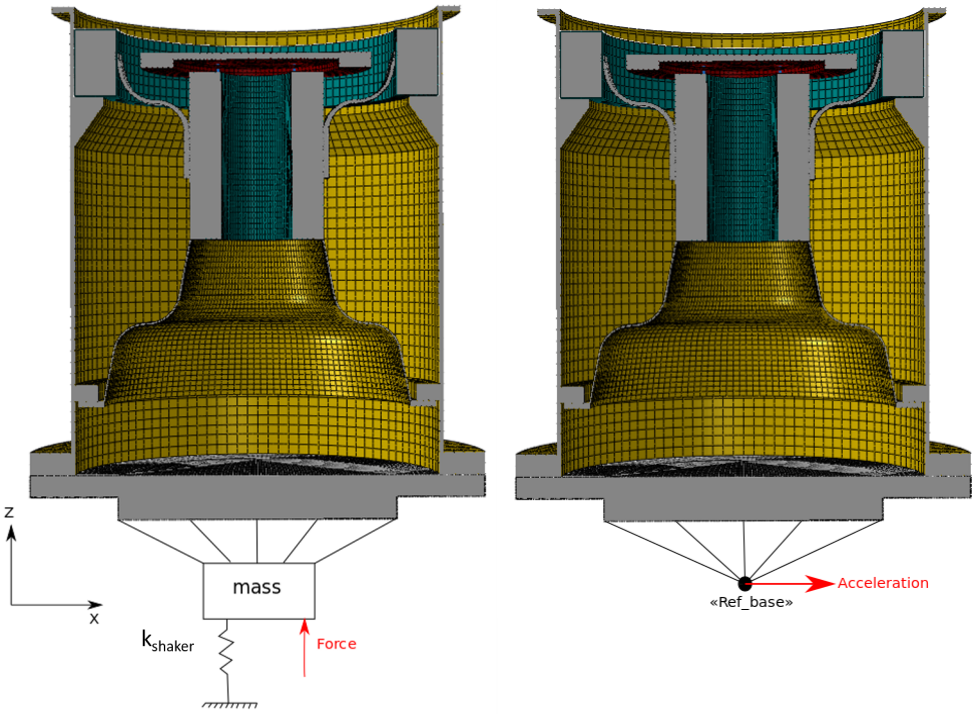

(a) (b)

Figure 5: Cross-section view of the finite-element model for (a)longitudinal excitations and (b) transverse excitations

4. Finite-Element Model of the structure Harmony-Gamma

4.1. Preamble

The structure has been modeled by means of the finite-element software ABAQUS. Figure 5 presents a cross-section view of the experimental assembly in two configurations: longitudinal excitation and transverse excitation. The base plate at the interface between the shaker and the structure is necessary only for the mounting of the longitudinal setting. It is also kept for the transverse setting, in order to work on a single finite-element model. This section presents the method and the choices of modeling for the different parts of the assembly and for the linear joints. Despite the conservation of the base plate between the two settings, the table configuration is modified, which imposes different limit conditions at the interface, depending on the setting. For the longitudinal setting, the mobile part of the shaker is modeled by a punctual inertial mass ($m_{\text{shaker}} = 15.88$ kg, according to the constructor data) with blocked transverse and rotational degrees of freedom. A spring with a stiffness $k_{\text{shaker}} = 22800$ N m limits the longitudinal movement of the punctual mass relative to the ground. The excitation is defined as a force applied on the punctual mass, which is legitimate due to the linear relation between intensity and force. The punctual mass is linked to the base plate by a structural coupling. The attached surface of the mass to the base plate needs to be updated in the model, since it drives the frequency of the third longitudinal resonance mode. For the transverse setting, the shaker is controlled to impose a transverse acceleration on the sliding table that holds the assembly. The excitation is applied through an acceleration term. The base plate is controlled by a reference node named "'Ref_base"' (see Figure 5b), kinematically coupled to the base plate. The movement of "'Ref_base"' is blocked in the directions x and y, and in rotation around the vertical axis z. The rotations around the axes x and y are not blocked, but rather controlled by springs whose stiffness needs to be updated. These parameters will allow the non-finite rotational inertia of the shaker to be taken into account.

The finite-element modeling of a blade is presented in Figure 6a. The reference nodes associated with the local system (x_{blade}, y_{blade}, z_{blade}) are specified in the figure. The blades are linked to the central body by means of two bolted screws, which are represented numerically by connectors between reference nodes. The connector stiffnesses are updated parameters that have a strong influence on the first longitudinal and transverse resonance modes. The connectors are rigid (with a stiffness of 10^{10} N m^{-1}) in directions x_{blade} and z_{blade}, and in rotation around y_{blade} and z_{blade}. Finite stiffnesses have been introduced in the direction y_{blade} and in rotation around the axis x_{blade}. Values for these two stiffnesses will be given in Section 4.2.

It is of paramount importance to keep the modeling as simple as possible, in order to be numerically

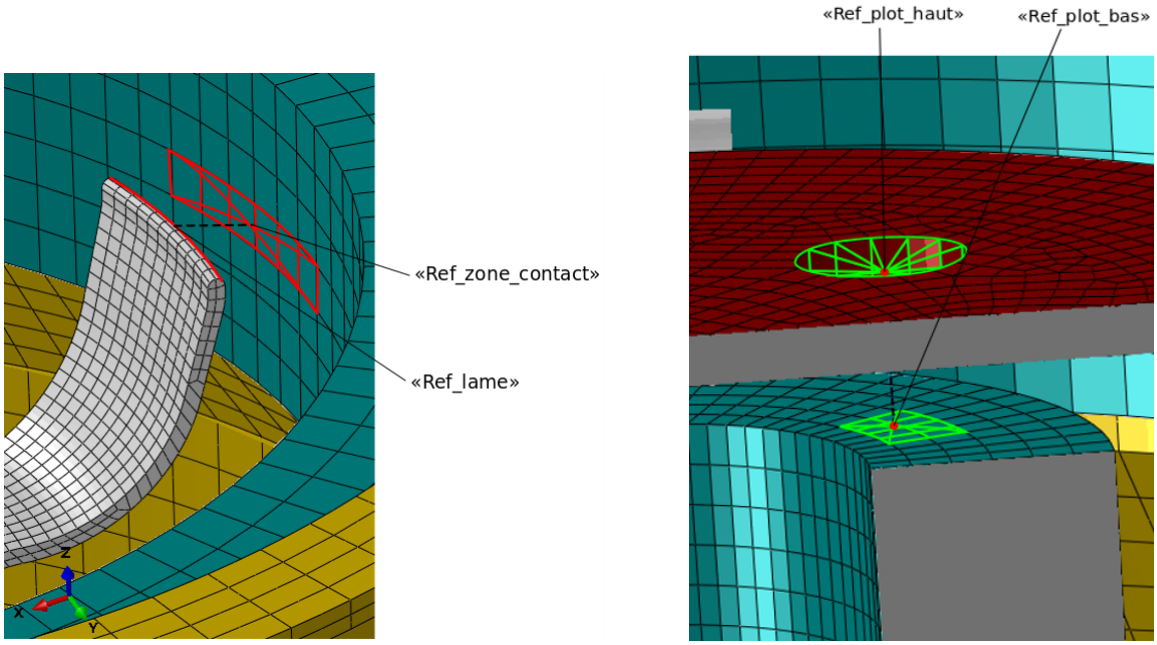

(a) (b)

Figure 6: Schema of the finite-element modeling of (a) a blade and (b) a rubber isolator

computable. In other words, the joint models must be as simple as possible and as accurate as necessary. Details regarding the nonlinear laws and their implementation are provided further on this document (see Sections 4.4.2 and 4.4.3).

4.2. Linear updating and validation

The underlying hypothesis of this first validation of the finite element model is that the nonlinearities are not active for low excitation levels, so experimental results can be compared to a linear model. For a model validation, a prior study of each part of the structure is conducted to individually update each of the sub-structures. These preliminary validations are not presented in the present work. For more details the reader can refer to [6]. Furthermore the finite element model of the structure Harmony which is identical to the structure Harmony-Gamma without the upper body and the four rubber isolators has been previously sutdy and validated in [6, 7]. More specifically, Claeys et al. [7] updated the friction joints stressed in the transverse direction for this structure Harmony in [7]. The updating yielded good correlations between experiments and simulations (less than 1% frequency error for the first two modes with a MAC criterion superior to 0.9, and 2.3% frequency error for the third mode with a MAC criterion equal to 0.87). The chosen updated parameters for the structure Harmony are kept for the present study [7]:

- the stiffness in the direction $\mathrm{y}_{\,\mathrm{blade}}$ and in rotation around $\mathrm{x}_{\,\mathrm{blade}}$ for the screws that link the blades to the central body. These two stiffnesses influence the first resonance frequency, but not the others. The updated values are $k_{\,\mathrm{screw\,y}} = 3\ 10^6$ N m^{-1} and $k_{\,\mathrm{screw}\,\theta\mathrm{x}} = 10^4$ N rad^{-1},
- the flexural stiffness of the sliding table, which is transposed as a rotational stiffness for the reference point "'Ref_Base"'. This stiffness influences the second resonance frequency. The updated value is $k_{\mathrm{Ref\_Base\ x}} = k_{\mathrm{Ref\_Base\ y}} = 3\ 10^7$ N rad^{-1}.

So in this present work the validation of the assembly model Harmony-Gamma (i.e. the previous validated structure Harmony plus the upper body and the four rubber isolators) is investigated. The inclusion of a elastomer joint model must be done in the finite element model. The global process that leads to the nonlinear modeling of the elastomer joint will be presented in Section 4.4.2. In the validation of the linear model of the structure Harmony-Gamma, the identification results of the elastomer joint at low excitation level are used (for more details see [8]).

Considering the validation of the finite element model Harmony-Gamma for the longitudinal modes, comparisons between experiments and simulations are undertaken at a low excitation level. Results are given in Figure 7. The overall excellent quality of the correlation over the entire frequency bandwidth (less than 1% frequency error for the 3 modes and a MAC criterion superior to 0.9 for each modes) enables the

validation of the linear updating and modeling of the finite element model of the structure Harmony-Gamma for longitudinal excitations. A cross-section view of the first three numerical longitudinal modes (denoted "'mode jL"' with j the mode number) is also provided in Figure 8.

Considering the validation of the finite element model Harmony-Gamma for the transverse modes, the first obtained results for the first four transverse modes (denoted "'mode jT"' with j the mode number) are presented in Table 2. These results have low quality, exhibiting frequency errors of 30% for resonance mode 4T, as well as bad spatial correlations. Due to the fact that the validation of the structure Harmony was previously done in [6, 7] for both the transverse and longitudinal excitations it implies that the problem necessarily comes from the modeling of the rubber isolators in transverse direction. In fact it appears that the attachment of the nonlinear elastomer joint is different between the mounting on the identification process of the elastomer properties [8] and the mounting on the structure Harmony-Gamma. Such differences between the two mountings, that have not been anticipated during the design of the structure Harmony-Gamma, are responsible of the poorly simulation prediction of the first four transverse modes. It can also be noted that these two different mountings attachments do not change the longitudinal dynamical behavior of the rubber isolator which explains the fact that the correlation for the longitudinal modes is excellent. A brief explanation is now proposed. The cross-section view of the rubber isolator is presented in Figure 9 for the two mounting configurations. Configuration 1 (left half of the schema) is used for the identification process of the nonlinear behavior of the elastomer joint, while Configuration 2 (right half of the schema) is used for the structure Harmony-Gamma. The main difference between the two configurations lies in the tightening at the end of the screw. For the first configuration, the tightening in ensured by a bolted joint tightened at 4 N m. For the second configuration, the tightening is ensured by a threading. The presence of a threading on the lower part of the rubber isolator implies that the central screw goes from one threaded hole directly to another. This does not ensure an efficient tightening of the elastomer joint. Consequently, the mounting of the elastomer joint for the structure harmony-Gamma is very flexible, and some of the transverse stress transits towards the central screw instead of transiting within the elastomer material. Hence, the elastomer joint has a much lower stiffness than that predicted by the identification process with Configuration 1. The nonlinear analysis that will be presented in Section 7.2 will be taken with caution and limited to qualitative results for transverse excitations. Nevertheless, a simple empirical modification of the elastomer model is proposed to obtain good agreement between experiments and numerical simulation for the first four transverse modes at low excitation level. So two empirical parameters α_T and α_L are added: the identified transverse (longitudinal, respectively) stiffness and damping of the rubber isolator with respect to the amplitude of displacement is multiplied by a coefficient $\alpha_T = 0.6$ (a coefficient $\alpha_L = 0.82$, respectively). Given that the transverse mode is experimentally softer than the numerical prediction, α_T is lower to 1. Moreover the updating of the longitudinal stiffness of the elastomer joint changes the third transverse mode 3T, which is a tilting of the upper body, soliciting both the longitudinal and the transverse directions of the rubber isolator. With the attachment mode of the rubber isolators on the structure Harmony-Gamma, only a part of the elastomer is solicited during the tilting of the upper body. This justifies the use of this updating parameter α_L, which is also bound to be lower than 1. A cross-section view of the first four numerical transverse modes (denoted "'mode jT"' with j the mode number) is provided in Figure 10. As indicated in Table 3, an overall good quality of the correlation is now obtained in the transverse direction: the first two modes modes 1T and 2T are still very well correlated, while modes 3T and 4T are now identified at a correct frequency, even though the spatial correlation remains quite poor. For the reader comprehension, Iit is also worth noting that the two values are realistic and coherent with the difference between the two mounting configurations of the elastomer joint. They indicates a more flexible behavior of the mounting for the elastomer joints of the structure Harmony-Gamma. The use of the two updated empirical parameters α_T and α_L will also be proposed in Section 7.2 to attempt to retrieve the principal nonlinear phenomena via calculation, and therefore to achieve a better understanding of these nonlinear phenomena. Finally Figure 11 shows a comparison between experiments and simulations for several accelerometers in the transverse direction over the entire frequency bandwidth. These results validate the linear updating with the two additional empirical parameters α_T and α_L, and the modeling of the finite element model of the structure Harmony-Gamma for transverse excitations.

4.3. Model reduction

The model presented in the previous section includes more than 300,000 degrees of freedom (DOFs). Nonlinear simulations are computationally expensive, which is incompatible with a detailed finite-element model. So the structure Harmony-gamma is reduced using a sub-structuring algorithm implemented in

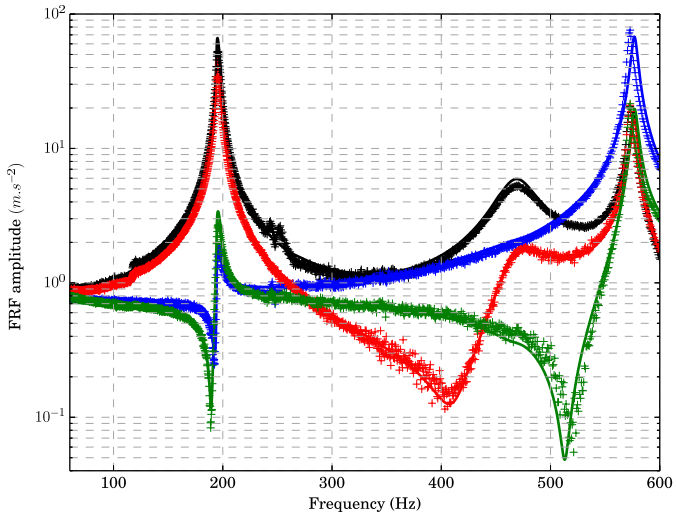

Figure 7: Experimental (crosses) and numerical (plain curves) frequency responses obtained for a longitudinal swept sine experiment of excitation level 162 N, at four measure points: upper body (black), central body (red), top of the envelope (blue) and base plate (green)

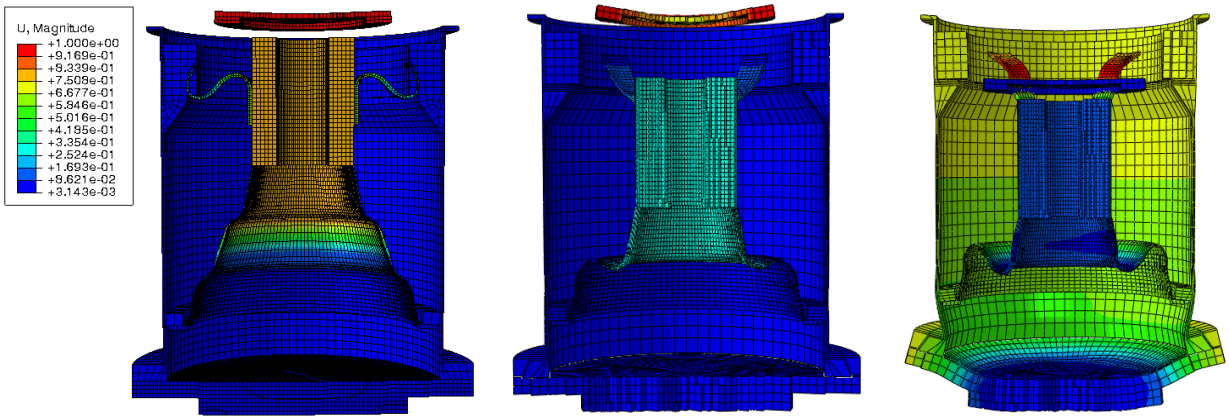

(a) (b) (c)

Figure 8: Cross-section view of longitudinal numerical modes of the assembly (a) mode 1L at 196 Hz , (b) mode 2L at 478 Hz and (c) mode 3L at 576 Hz

Abaqus [9] that is a variant of the Hurty or Craig–Bampton methods [10, 11]. For the interested reader this method has been previously used and presented in [6] and a review of the most popular widely used Component Mode Synthesis methods can also be found in [12].

First of all, the following physical DOFs of the structure Harmony-Gamma are kept:

- the DOFs x, y and z of the closest node to the 11 accelerometers. These physical DOFs allow a direct comparison between the results obtained on the reduced basis and the experimental results. Thisd corresponds to a total of 33 DOFs.
- the vertical DOF of the inertial mass for the longitudinal setting. The excitation force will be applied on this DOF. This DOF is not kept for the transverse setting.
- the nonlinear friction and elastomer joints have a peculiar treatment. It is of paramount importance

Mode number	Numerical frequency (Hz)	Frequency error versus experiments	Spatial correlation (MAC)
1T	98.99	0.95%	0.99
2T	191.1	3.87%	0.93
3T	272.7	6.74%	0.66
4T	452.5	31.5%	0.45

Table 2: Initial comparison of the numerical and experimental resonance modes of the structure Harmony-Gamma under transverse excitation

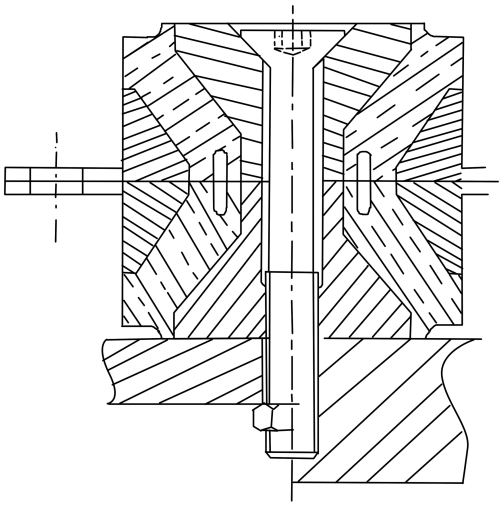

Figure 9: Cross-section view of the rubber isolator with the two configurations. Configuration 1 (left half of the schema) is used for the identification process of the rubber isolator, while Configuration 2 (right half of the schema) is used for the structure Harmony-Gamma

Mode number	Numerical frequency (Hz)	Frequency error versus experiments	Spatial correlation (MAC)
1T	97.9	-0.15%	0.99
2T	189.8	3.17%	0.96
3T	247.9	-2.61%	0.66
4T	355.5	3.29%	0.58

Table 3: Comparison between the numerical and experimental resonance modes of the structure Harmony-Gamma under transverse excitation by isnug the empirical update of the rubber isolators

for further nonlinear calculations to be able to compute the internal stress of these joints, which is possible with this sub-structuring method on condition that certain DOFs are retained. For each of the four friction blades, the six DOFs of the reference nodes "'Ref_contact_zone"', "'Ref_screw_1"' and "'Ref_screw_2"' (see Figure 6a) are kept. The reference nodes "'Ref_blade"' are voluntarily excluded in order to improve the convergence of the calculations. Details regarding this delicate matter are discussed in [6]. A total of 72 DOFs are kept for the friction joints of the blades. With regard to the rubber isolators, a total of 48 DOFs are kept (i.e. 6 DOFs for each of the reference nodes "'Ref_elastomer_bottom"' and "'Ref_elastomer_top"').

Besides these physical DOFs, the modal vectors are retained for the assembly and introduced into the reduced basis. The study is limited to the modes contained within the frequency bandwidth [5;1000] Hz, which corresponds to 15 modes. The substructuring method ensures the accuracy of the modes between the reduced basis and the complete basis. Finally, the size of the reduced model is 169 for the longitudinal

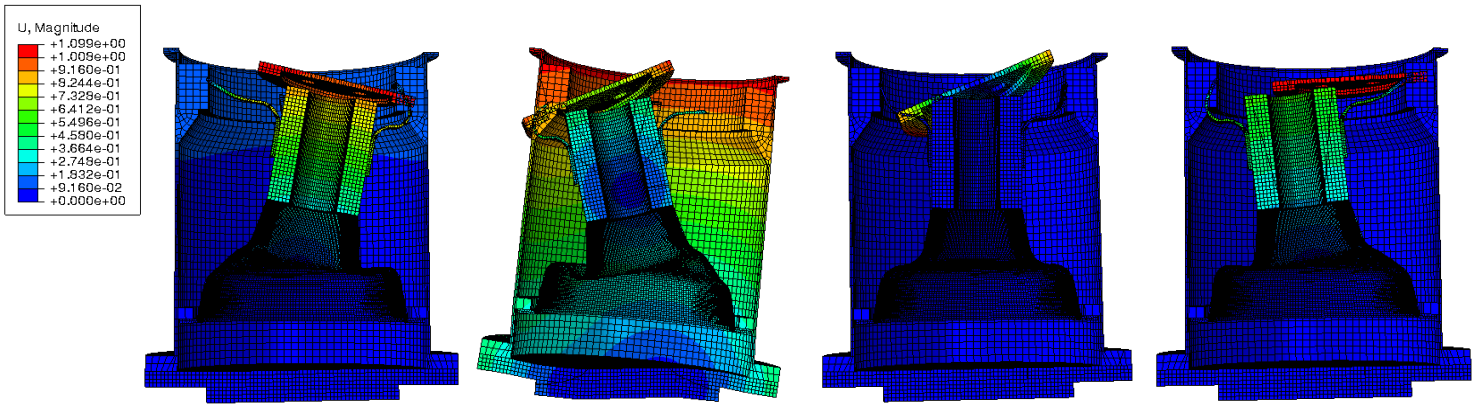

(a) (b) (c) (d)

Figure 10: Cross-section view of the transverse numerical modes of the assembly (a) mode 1T (b), mode 2T (c), mode 3T (d) and mode 4T

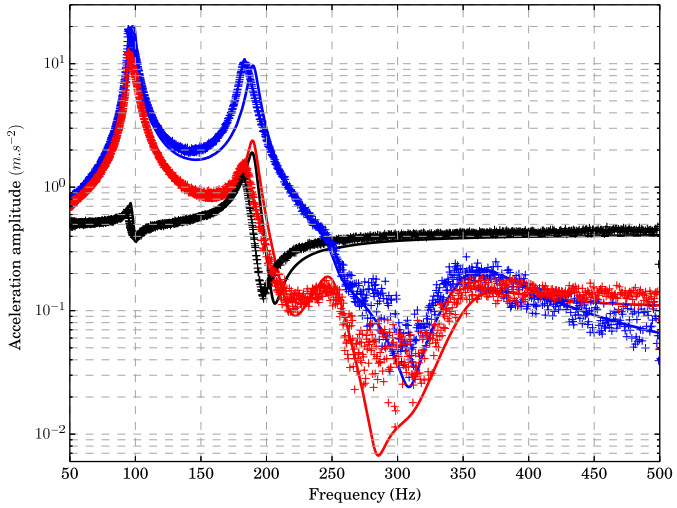

Figure 11: Experimental (crosses) and numerical (plain curves) frequency responses with a transverse swept sine experiment at 0.5 m s^{-2}, at three measure points: upper body (blue), central body (red) and base plate (black)

setting and 168 for the transverse setting, which leads to a significant reduction in the size of the problem to be treated. Before the introduction of the nonlinear friction and elastomer joints, the dynamical equation for the structure Harmony-Gamma is written in the reduced basis as:

$$\mathbf{M}\ddot{\mathbf{x}} + \mathbf{D}\dot{\mathbf{x}} + \mathbf{K}\mathbf{x} = \mathbf{F}_{\mathbf{excit}}(t) \tag{1}$$

where $\mathbf{x}$ is the displacement vector in the reduced basis. $\mathbf{M}$, $\mathbf{D}$ and $\mathbf{K}$ are the matrices of mass, damping and stiffness respectively, and $\mathbf{F}_{\mathbf{excit}}$ is the projection of the excitation vector in the reduced basis. $\mathbf{D}$ is a linear damping matrix built through an experimental identification process. This matrix will be useful to describe the damping at low excitation levels when the nonlinearities are inactive. For high excitation levels, nonlinearities will be responsible for most of the damping, and the linear damping matrix will have a negligible impact on the response. For longitudinal excitations, three resonance modes are observed in the frequency bandwidth [5-1000] Hz. The identification process is achieved at a low excitation level, in order to limit the activation of the nonlinearities. The introduction of nonlinear stiffness and damping into the model will be presented in the next section, and it will be shown that the damping of the rubber isolators drives the damping of the second resonance mode. Therefore, a Rayleigh procedure is used to update the damping of Modes 1 and 3, such as $\mathbf{D} = \alpha\mathbf{M} + \beta\mathbf{K}$ with $\alpha = 0.5\ 10^{-2}$ and $\beta = 9.35$. The same process is used for the transverse setting, where four modes have been identified. A Caughey process is applied for the three first modes. In the end, $\mathbf{D} = \mathbf{M}\left(\sum_{k=0}^{3-1} a_k\,(\mathbf{M}^{-1}\mathbf{K})^k\right)$, with $a_0 = 8.87$, $a_1 = 2.79\ 10^{-5}$ and $a_2 =$ -2.59 10^{-12}. The damping of the fourth mode is driven by the damping of the rubber isolators that will be introduced in the nonlinear force.

4.4. Introduction of the nonlinear modeling

The introduction of a friction model for the blades or a viscoelastic model for the elastomer is achieved by replacing a linear rigid connector by a nonlinear friction or elastomer joint, respectively. This section details the process of replacement of the linear joints by nonlinear friction or elastomer joints inside the reduced matrices, and also presents the different nonlinear modeling used. First, the methodology to apply a nonlinear force on the structure Harmony-Gamma is briefly presented. This methodology has been presented in [6]. Secondly, the two nonlinear models are presented, respectively for the rubber isolators and the friction blades.

4.4.1. Definition of the application vector of the nonlinear force

In the final nonlinear finite element model of the structure Harmony-Gamma, the linear joints are replaced by nonlinear friction or elastomer joints simply by deducing the stiffness of the linear joint to the global stiffness matrix:

$$\mathbf{K}_{\mathbf{c.m.}} - k_{\text{joint c.m.}}\mathbf{V}_{\mathbf{joint\ c.m.}}{}^{T}\mathbf{V}_{\mathbf{joint\ c.m.}} = \mathbf{K}_{\mathbf{no\ joint\ c.m.}} \tag{2}$$

where c.m. stands for complete model. $\mathbf{V_{joint\,c.m.}}$ is the joint vector in the complete basis, with only two non-null components associated with the nodes of the joint, with values 1 and -1. Let $[\mathbf{\Psi_r}, \mathbf{\Phi_p}]$ be the reduction basis of the substructuring method, with $\mathbf{r}$ the retained DOFs and $\mathbf{p}$ the retained modes. The stress in the nonlinear friction or elastomer joint is calculated in two different ways, depending on whether the reference nodes of the joint are all retained in the reduced basis, or not.

When all of the reference nodes of the joint are retained (which is the case for the rubber isolators), the modeling of the elastomer joint in the reduced basis can be simply written as follows:

$$\mathbf{F_{joint\,elastomer}}(\mathbf{x}) = k_{\text{joint m.c.}} \mathbf{V_{joint}}^T \mathbf{V_{joint}}\,\mathbf{x} \tag{3}$$

with $\mathbf{V_{joint}} =^T [\mathbf{\Psi_r}, \mathbf{\Phi_p}]\mathbf{V_{joint\,c.m.}}$. In that case, the models of the joint are independent from one another and the total force in the joints is written as the sum of the internal forces:

$$\mathbf{F_{joints\,elastomer}}(\mathbf{x}) = \sum_j k_{\text{joint c.m. j}} \mathbf{V_{joint\,j}}^T \mathbf{V_{joint\,j}}\mathbf{x} \tag{4}$$

When the nodes are not all retained in the joint (which is the case for friction joint of the blades), then the calculation of the internal stress becomes more complex. Four virtual reference points "'Ref joint j"' are first introduced, since there are a total of four blades. The movement of "'Ref joint j"' is driven by the equation:

$$x_{\text{Ref joint j}} = x_{\text{Ref contact zone j}} - x_{\text{Ref blade j}} \tag{5}$$

Then a loading case for each of the virtual points on ABAQUS is compute. Let $\mathbf{V_{liaison\,j}}^*$ be these loading cases, it is then possible to define a set of joints:

$$\mathbf{V_{joint\,k}} = \mathbf{V_{joint\,k}}^* - \sum_{j=1}^{k-1} \left(\frac{k_{\text{joint j c.m.}}}{k_{\text{joint k c.m.}}} \right) \left(\frac{\mathbf{V_{joint\,j}}|\,\text{Ref contact zone k}}{\mathbf{V_{joint\,j}}|\,\text{Ref contact zone j}} \right) \mathbf{V_{joint\,j}} \tag{6}$$

$$k_{\text{joint k}} = \frac{k_{\text{joint k c.m.}}}{\mathbf{V_{joint\,k}}|\,\text{Ref contact zone k}} \tag{7}$$

where "'$\mathbf{V_{joint\,i}}|$ Ref contact zone j"' is the value of the vector $\mathbf{V_{liaison\,i}}$ on the reference node "' Ref contact zone j"'. With these definitions, the joint models can be treated independently and summed:

$$\mathbf{F_{joints}}(\mathbf{x}) = \sum_j k_{\text{joint j}}\, u_{\text{j}} \mathbf{V_{joint\,j}} \tag{8}$$

where $u_{\text{j}} =^T \mathbf{V_{joint\,j}}\mathbf{x}$.

4.4.2. Elastomer modeling

Modeling elastomers proves difficult, since rubber materials follow complex physical laws with mechanical properties, e.g. dynamic hardness and damping, that are dependent not only on fillers in the material, but also on temperature, frequency and the amplitude of the motion. Nonlinearities in an elastomer joint are discussed by Harris and Stevenson [13]. Explanations on the underlying physical mechanisms are provided in [14]. Different methodologies have been developed in the past in the literature to study and to characterize the behavior of rubber isolators. First, methods based on the modeling of the mechanical laws of the elastomer, using physical models such as the Kelvin-Voigt or Maxwell model [15], fractional derivatives [16], or the Berg model [17], to name just a few. A more recent approach by Jalocha et al. [18] uses Dynamic Mechanical Analysis(DMA) tests to characterize materials and to create a prestrain-dependent viscoelastic constitutive model. The accurate physical model respects the laws of thermodynamics, and is based on only three parameters to update, achieving excellent agreement with the experiments. These methods are usually precise, but require complex modeling of the joint, through a finite-element discretization of the latter [5, 19**?**]. The second class of methods is based on phenomenological modeling integrated at the scale of the mechanism, and will be used in this study. They take the form of a one-degree-of-freedom system whose stiffness and damping are polynomial [20] or exponential [21] of the relative displacement of the mechanism. The approach used in the present work is based on this phenomenological modeling of the elastomer joint by a one-degree-of-freedom mechanism, whose properties are only amplitude-dependent (Payne effect).

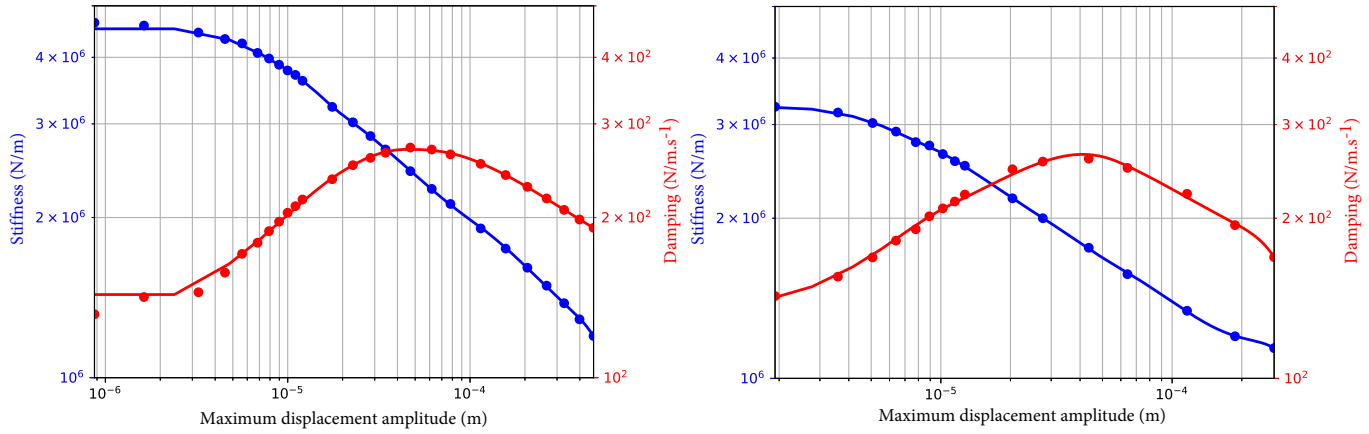

(a) (b)

Figure 12: Evolution of the identified stiffness (blue) and damping (red) with respect to the displacement amplitude for (a) longitudinal excitation and (b) transverse excitation

The uni-axial behavior of the elastomer joint is identified using swept-sine experiments with increasing excitation levels. The schematic cross-section view of one rubber isolator used for the identification process is shown in Figure 9. The identification procedure is carried out in laboratory for a longitudinal (transverse, respectively) excitation in order to recover the longitudinal (transverse, respectively) behavior of the rubber isolator. For more details, the complete identification process is fully explained and discussed in [8]. The stiffness and damping evolutions with respect to the displacement amplitude are presented in Figures 12 for both the longitudinal and transverse behaviors of one rubber isolator.

As explained in Section 4.4.1, the nonlinear force replaces the linear force:

$$\mathbf{F_{nl,\,joint}}(u_i) = (k_{\,\text{joint}}\, u_i - f_i)\mathbf{V_{joint}} \tag{9}$$

where u_i is the axial deformation of the elastomer joint, $k_{\,\text{joint}}$ is the linear stiffness of the elastomer joint in the reduced basis and f_i is the nonlinear force of the elastomer joint calculated by

$$f_i = K(u_i)u_i + D(u_i)\dot{u}_i \tag{10}$$

K and D are the stiffness and damping functions that are identified experimentally. A set of nonlinear values has been updated for the longitudinal displacement of the elastomer (DOF z) and another set of nonlinear values has been updated for the transverse displacement (DOF x and y). In this application, the structure Harmony-Gamma is composed of four rubber isolators. For each one, the nonlinearity can be activated along three directions: longitudinal ($\text{z}_{\,\text{elastomer}}$) and transverse ($\text{x}_{\,\text{elastomer}}$ and $\text{y}_{\,\text{elastomer}}$). For longitudinal simulations, the only nonlinear components of the rubber isolator are the stiffness and damping of the $\text{z}_{\,\text{elastomer}}$ axis. A priori, there is no parameter to update since the model has been validated experimentally for one rubber isolator. However, the different operating conditions of temperature and the dispersion of the rubber isolators' properties lead to the introduction of an updating parameter as previously explained in Section 4.2. More details will also be given in Section 7.1. For transverse experiments along the Y axis, the components of the $\text{z}_{\,\text{elastomer}}$ axis and $\text{x}_{\,\text{elastomer}}$ axis are kept, for a total of 8 nonlinear DOFs and there is no parameter to update *a priori*.

4.4.3. Friction modeling

The modeling of nonlinear friction joints is still a current a research topic of interest for researchers working in the field of structural dynamic. Different empirical friction models have been proposed and developed in order to give a better description of friction joint mechanics and to improve prediction capabilities of nonlinear dynamics of mechanical systems [22, 23, 24, 25, 26, 27, 28, 29, 30]. The goal of such models is to capture the energy dissipation during friction events accurately in order to predict the overall forced responses of mechanical systems with friction joints. For the interested reader, a recent overview of constitutive models of friction is proposed in [31]. In the present work, a Jenkins modeling is chosen for the friction that occurs at the interface between the blades and the envelope. This model is represented in Figure 13a. It is composed of a linear spring in series with a Coulomb friction model. Sliding occurs when

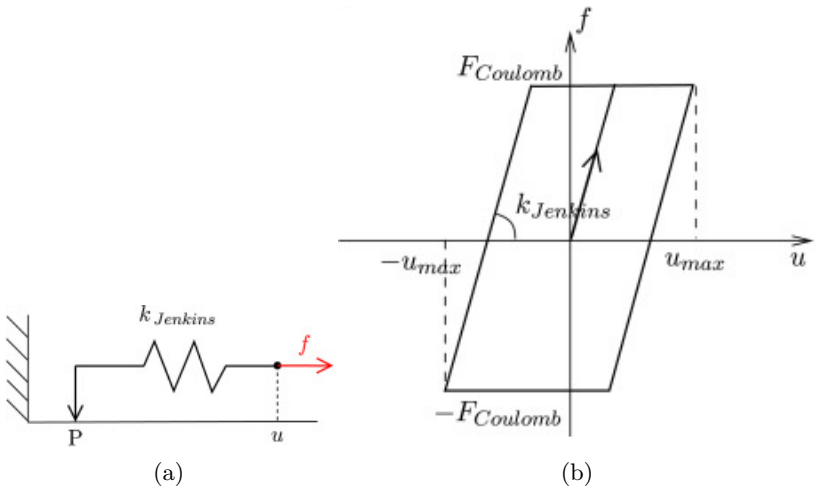

(a) (b)

Figure 13: Friction modeling (a) Jenkins model and (b) force / displacement Coulomb law

the force f in the friction joint exceeds the friction threshold F_{Coulomb}. Then, the sliding is such that the force f in the nonlinear friction joints is equal to the Coulomb threshold. There are therefore two phases:

- an adhesion phase where $|f| < F_{\text{Coulomb}}$ and the point P of the interface is motionless $v_P = 0$,
- a sliding phase where $|f| = F_{\text{Coulomb}}$ and $v_P = \dot{u}$.

The force / displacement diagram of this Coulomb law is presented in Figure 13b for a periodic movement. The calculation of the internal stress of the friction joint is a two step procedure, based on an iterative formulation initially proposed by Guillen and Pierre [32]. For each temporal iteration i, it is first assumed that the Coulomb joint is in the adhesion phase between the state $i-1$ and i. A virtual force ${}^{vir}f$ is then calculated:

$$ {}^{vir}f = f_{i-1} + k_{\text{joint}}(u_i - u_{i-1}) \tag{11} $$

If the virtual force is inferior to the threshold, the force in the friction joint is equal to this virtual force and the friction joint stays in an adhesion phase. If the virtual force is beyond the Coulomb threshold, then the friction joint enters into a sliding phase, and the force is equal to the Coulomb threshold:

$$ f_i = \begin{cases} {}^{vir}f & \text{if } |{}^{vir}f| < F_{\text{Coulomb}} \quad \text{(adhesion)} \\ \text{sgn}({}^{vir}f)\, F_{\text{Coulomb}} & \text{if } |{}^{vir}f| \geq F_{\text{Coulomb}} \quad \text{(slide)} \end{cases} \tag{12} $$

The expression of the nonlinear vectorial force are finally given by

$$ \mathbf{F_{nl,\,joint}}(u_i) = (k_{\text{joint}}\, u_i - f_i)\mathbf{V_{joint}} \tag{13} $$

The structure Harmony-Gamma is composed of four contact blades. For each contact, friction can occur along three directions: longitudinal (z_{blade}), transverse (y_{blade}) or in rotation around the x_{blade} axis. Only the components in the z_{blade} axis are retained for longitudinal excitations (for a total of 4 nonlinear elements). For transverse excitations, the proposed approach is based on Claeys's results [6]. Friction first occurs in rotation around x_{blade} and in translation along the x_{blade} axis for the two blades whose top is collinear to the excitation. Then, at higher excitation levels, friction may also occur in the two other blades along the z_{blade} axis. Consequently, a total of 6 nonlinear elements are retained for a transverse excitation, with three updating parameters: $\text{F}_{\text{Coulomb, }\theta\text{y}}$, $\text{F}_{\text{Coulomb, x}}$ and $\text{F}_{\text{Coulomb, z}}$.

5. Numerical method for nonlinear simulations

The frictional and elastomer models are nonlinear and require specific methods to compute the nonlinear responses for harmonic excitations. In the present study, the stationary harmonic solution of the system is sought. The well known Harmonic Balance Method [1] is used to compute the stationary solution of the nonlinear problem. This method is coupled with a continuation method to describe the solution space continuously. In order to limit the computational time of the nonlinear method, a condensation procedure [33, 34] is introduced to reduce the size of the nonlinear problem.

5.1. Harmonic Balance Method

The nonlinear dynamical equation of the structure Harmony-Gamma can eventually be written as:

$$\mathbf{M}\ddot{\mathbf{x}} + \mathbf{D}\dot{\mathbf{x}} + \mathbf{K}\mathbf{x} = \mathbf{F_{excit}}(t) + \sum_{joint} \mathbf{F_{nl,joint}}({}^{T}\mathbf{V_{joint}}\,\mathbf{x}) = \mathbf{F_{excit}}(t) + \mathbf{F_{nl}}(t) \tag{14}$$

where $\mathbf{F_{nl,joint}}$ includes all of the nonlinear joints of the rubber isolators and friction blades.

In the present study the input excitation is harmonic (i.e. $\mathbf{F_{excit}}(t) = \mathbf{C_{1,excit}}\cos(\,\Omega t)$). So the displacement vector, the nonlinear source term are assumed to be approximated by a finite Fourier series with Ω as a fundamental frequency:

$$\mathbf{x}(t) = \mathbf{B_0} + \sum_{k=1}^{N} \mathbf{A_k}\sin(k\Omega\, t) + \mathbf{B_k}\cos(k\,\Omega t) \tag{15}$$

$$\mathbf{F_{nl}}(t) = \mathbf{C_0} + \sum_{k=1}^{N} \mathbf{S_k}\sin(k\,\Omega t) + \mathbf{C_k}\cos(k\,\Omega t) \tag{16}$$

N, the order of the Fourier series, is selected on the basis of the number of significant harmonics expected in the nonlinear dynamical response. For the present study N is chosen equal to 1. Usually, a higher number of harmonics is desired in the response, however, the nonlinear description of the elastomer is such that the elastomer nonlinear force is non-null only on the first harmonic.

The general nonlinear equation may be written in the Fourier domain:

$$\mathbf{A}\mathbf{X} = \mathbf{B_{excit}} + \mathbf{B_{nl}} \tag{17}$$

with

$$\mathbf{A} = \mathrm{Diag}\left(\mathbf{K}, \left\{ \begin{bmatrix} \mathbf{K} - (k\Omega)^2\mathbf{I_d} & -k\Omega\mathbf{D} \\ k\Omega\mathbf{D} & \mathbf{K} - (k\Omega)^2\mathbf{I_d} \end{bmatrix} \right\}_{k=1,\ldots,N}\right) \tag{18}$$

$$\mathbf{X} = {}^{T}[\mathbf{B_0},\, \mathbf{A_1},\, \mathbf{B_1}, \ldots,\, \mathbf{A_N},\, \mathbf{B_N}] \tag{19}$$

$$\mathbf{B_{excit}} = {}^{T}[\mathbf{0},\, \mathbf{0},\, \mathbf{C_{1,excit}},\, \mathbf{0},\, \ldots,\, \mathbf{0}] \tag{20}$$

$$\mathbf{B_{nl}} = {}^{T}[\mathbf{C_0},\, \mathbf{S_1},\, \mathbf{C_1},\, \ldots,\, \mathbf{S_N},\, \mathbf{C_N}] \tag{21}$$

The size of the system is $(2N+1)n$ where n is the number of DOFs retained during the reduction procedure. The nonlinear coefficients of $\mathbf{B_{nl}}$ can be calculated by applying the classical Alternating Frequency Time domain method (AFT-method) [35].

5.2. Condensation process based on the separation of linear and nonlinear DOFs

5.2.1. Condensation procedure

A condensation procedure similar to that proposed by Sinou [34] is introduced to reduce the size of the nonlinear problem, and thus the computational time. This condensation procedure consists in a basis change that separates the vectors into vectors with applied linear and nonlinear forces, and vectors with linear force only. This separation is possible in the particular case of localized nonlinearities. Given that the nonlinearity is local (in the contact region for the friction blades, or at the interface between the upper body and the central body for the rubber isolators), most of the DOFs are not affected by the nonlinear source terms and are thus related to other DOFs through linear relations. So the condensation procedure is based on a substitution process: it aims at separating these two kinds of DOFs (affected or non-affected by the nonlinear source terms) to reduce the size of the problem to the number of DOFs affected by the nonlinear force. In this application, a maximum of 12 nonlinear DOFs would be kept.

Let q be the number of application vectors of the nonlinear forces. These q vectors $\{\mathbf{V_{joint,i}}\}_{i=1,\ldots,q}$ are chosen to be the first vectors of the new base. These application vectors can be retrieved through the substructuring with ABAQUS. The new basis is obtained by applying the Gram-Schmidt orthonormalization

algorithm to the family of vectors $\{\mathbf{V_i}\}_{i=1,...,n+q} = \{\{\mathbf{V_{liaison,\,i}}\}_{i=1,...,q}, [\mathbf{I_d}]_n\}$. The vectors of the basis are built iteratively following the schema:

$$\begin{aligned}
\widetilde{\mathbf{V}}_\mathbf{1} &= \frac{\mathbf{V_1}}{\|\mathbf{V_1}\|} \\
&... \\
\widetilde{\mathbf{V}}_\mathbf{i} &= \frac{\mathbf{V_i} - \sum_{j=1}^{i-1} (\mathbf{V_i}|\widetilde{\mathbf{V}}_\mathbf{j})\, \widetilde{\mathbf{V}}_\mathbf{j}}{\left\| \mathbf{V_i} - \sum_{j=1}^{i-1} (\mathbf{V_i}|\widetilde{\mathbf{V}}_\mathbf{j})\, \widetilde{\mathbf{V}}_\mathbf{j} \right\|}
\end{aligned} \tag{22}$$

where $(.|.)$ represents the scalar product in R^n.

Eventually, the null vectors are eliminated and an orthonormal basis $\widetilde{\mathbf{V}} = \{\widetilde{\mathbf{V}}_\mathbf{i}\}_{i=1,...,n}$ is formed. In this new basis, the application vectors only depend on the first q vectors of the basis:

$$\mathbf{V_{liaison\,i}} = \sum_{j=1}^{i-1} (\mathbf{V_{liaison\,i}}|\widetilde{\mathbf{V}}_\mathbf{j})\widetilde{\mathbf{V}}_\mathbf{j} + \left\| \mathbf{V_{liaison\,i}} - \sum_{j=1}^{i-1} (\mathbf{V_{liaison\,i}}|\widetilde{\mathbf{V}}_\mathbf{j})\widetilde{\mathbf{V}}_\mathbf{j} \right\| \widetilde{\mathbf{V}}_\mathbf{i} \qquad \forall\, i \in [1; q] \tag{23}$$

The nonlinear forces are only applied on these q application vectors, which will be mentioned as the nonlinear DOFs of the system. Conversely, the next $p = n - q$ vectors are called the linear DOFs of the system. The new basis enables a separation between the linear and the nonlinear DOFs:

$${}^T\widetilde{\mathbf{V}}\,\mathbf{x} = \begin{bmatrix} \mathbf{x_q} \\ \mathbf{x_p} \end{bmatrix} \tag{24}$$

$$\mathbf{^T\widetilde{V}M\widetilde{V}}\,\ddot{\mathbf{x}} + \mathbf{^T\widetilde{V}D\widetilde{V}}\,\dot{\mathbf{x}} + \mathbf{^T\widetilde{V}K\widetilde{V}}\,\mathbf{x} = \mathbf{^T\widetilde{V}F_{excit}}(t) + \begin{bmatrix} \mathbf{F_{nl}(x_q)} \\ \mathbf{0} \end{bmatrix} \tag{25}$$

The following matrix Λ is also defined in order to minimize the size of the nonlinear optimization system in the Fourier basis :

$$\Lambda = [\mathbf{I_{2N+2}} \otimes \widetilde{\mathbf{V}}_\mathbf{q} | \mathbf{I_{2N+2}} \otimes \widetilde{\mathbf{V}}_\mathbf{p}] \quad \text{with} \quad \widetilde{\mathbf{V}}_\mathbf{q} = \{\widetilde{\mathbf{V}}_\mathbf{i}\}_{i=1,...,q}\,, \quad \widetilde{\mathbf{V}}_\mathbf{p} = \{\widetilde{\mathbf{V}}_\mathbf{i}\}_{i=q,...,n} \tag{26}$$

where $\otimes$ defines the classical Kronecker product and $\mathbf{I}$ corresponds to the identity matrix. This matrix Λ corresponds to the basic change in the Fourier basis in connection with the previous condensation procedure (that aims at separating DOFs affected or non-affected by the nonlinear source term). By introducing the following notations

$${}^T\Lambda\mathbf{X} = \begin{bmatrix} \mathbf{X_q} \\ \mathbf{X_p} \end{bmatrix} \quad {}^T\Lambda\mathbf{A}\Lambda = \begin{bmatrix} \mathbf{A_{qq}} & \mathbf{A_{qp}} \\ \mathbf{A_{pq}} & \mathbf{A_{pp}} \end{bmatrix} \quad {}^T\Lambda\mathbf{B_{excit}} = \begin{bmatrix} \mathbf{B_{excit,\,q}} \\ \mathbf{B_{excit,\,p}} \end{bmatrix} \tag{27}$$

Equation (17) can be rewritten in the new basis as follows:

$$\begin{bmatrix} \mathbf{A_{qq}} & \mathbf{A_{qp}} \\ \mathbf{A_{pq}} & \mathbf{A_{pp}} \end{bmatrix} \begin{bmatrix} \mathbf{X_q} \\ \mathbf{X_p} \end{bmatrix} = \begin{bmatrix} \mathbf{B_{excit,\,q}} \\ \mathbf{B_{excit,\,p}} \end{bmatrix} + \begin{bmatrix} \mathbf{B_{nl}(X_q)} \\ \mathbf{0} \end{bmatrix} \tag{28}$$

By construction, the nonlinear force is only applied on the nonlinear vectors, and $\mathbf{B_{nl}(X_p)} = \mathbf{0}$. The previous equation enables the establishment of a linear relation between $\mathbf{X_p}$ and $\mathbf{X_q}$:

$$\mathbf{X_p} = \mathbf{A_{pp}}^{-1} \left(\mathbf{B_{excit,\,p}} - \mathbf{A_{pq}X_q}\right) \tag{29}$$

Replacing $\mathbf{X_p}$ by this expression within Equation (28), the nonlinear equation of dimension $(2N+1)q$ is obtained:

$$\left(\mathbf{A_{qq}} - \mathbf{A_{qp}A_{pp}}^{-1}\mathbf{A_{pq}}\right)\mathbf{X_q} = \mathbf{W_{excit,\,q}} - \mathbf{A_{qp}A_{pp}}^{-1}\mathbf{W_{excit,\,p}} + \mathbf{W_{nl}(X_q)} \tag{30}$$

This is the nonlinear system of equations of size $(2N+1)q$ that will be solved, instead of the initial system of size $(2N+1)(p+q)$. Once $\mathbf{X_q}$ is known, the solution $\mathbf{X}$ of the problem (17) is computed by applying Equations (27) and (29):

$$\mathbf{X} = \mathbf{\Lambda} \begin{bmatrix} \mathbf{X_q} \\ \mathbf{A_{pp}}^{-1} \left(\mathbf{W_{excit,\,p}} - \mathbf{A_{pq}X_q}\right) \end{bmatrix} \tag{31}$$

5.2.2. Alternate Frequency Time Method in the condensed Fourier space

The relation $\mathbf{B_{nl}}(\mathbf{X_q})$ is computed through an Alternate Frequency Time method in the condensed Fourier space. Firstly, an inverse Fourier Transform is used on the nonlinear vector $\mathbf{X_q}$ to transition from the Fourier domain to the temporal domain:

$$\{\mathbf{x_q}\}_i(t) = \{\mathbf{B_0}\}_i + \sum_{k=1}^{N} \{\mathbf{A_k}\}_i \sin(k\,\Omega t) + \{\mathbf{B_k}\}_i \cos(k\,\Omega t) \qquad \forall\, i \in [1; q] \tag{32}$$

where $\{\mathbf{A_k}\}_i$ and $\{\mathbf{B_k}\}_i$ are the k^{th} Fourier coordinates of the i^{th} vector term $\mathbf{X_q}$. From these displacements the elongations of each joint $u_{\,liaison,\,i} = {}^{T}\mathbf{V_{liaison,\,i}}\,\mathbf{x}$ is deduced by considering Equation (23):

$$u_{\,joint\,i}(t) = \sum_{j=1}^{i-1} (\mathbf{V_{joint\,i}} | \widetilde{\mathbf{V}}_\mathbf{j}) \{\mathbf{x_q}\}_j(t) + \left\| \mathbf{V_{joint\,i}} - \sum_{j=1}^{i-1} (\mathbf{V_{joint\,i}} | \widetilde{\mathbf{V}}_\mathbf{j}) \widetilde{\mathbf{V}}_\mathbf{j} \right\| \{\mathbf{x_q}\}_i(t) \tag{33}$$

The nonlinear force of each joint can then be computed:

$$\mathbf{F_{nl\,joint,\,i}} = (k_{joint\,i} u_{joint\,i} - f_{nl\,joint}(u_{joint\,i}))\mathbf{V_{joint\,i}} \tag{34}$$

Then, a summation of the contributions of each joint i is performed:

$$\mathbf{F_{nl}}(\mathbf{x_q}(t)) = \sum_{i=1}^{q} \mathbf{F_{nl\,joint\,i}}(\mathbf{x_q}(t)) \tag{35}$$

Once this nonlinear force has been computed in the temporal domain, it is switched back into the Fourier domain with a direct Fourier Transform. Equation (30) can then be considered as a nonlinear optimization problem given by:

$$\mathbf{H}(\mathbf{X_q}) = \left(\mathbf{A_{qq}} - \mathbf{A_{qp}}{\mathbf{A_{pp}}}^{-1}\mathbf{A_{pq}}\right)\mathbf{X_q} - \mathbf{B_{excit,\,q}} - \mathbf{A_{qp}}{\mathbf{A_{pp}}}^{-1}\mathbf{B_{excit,\,p}} + \mathbf{B_{nl}}(\mathbf{X_q}) = \mathbf{0} \tag{36}$$

Finally the problem (36) is solved using a continuation procedure, to obtain a continuous response curve in the frequency domain. A predictor-corrector scheme has also been implemented [1]. The Newton-Raphson continuation method is chosen.

6. Preliminary numerical analysis to the effects of the friction and elastomer joints

Before presenting the different comparisons between experiments and simulations, a prior analysis is proposed to understand the role of each nonlinearity in the structural response. Longitudinal swept sine simulations will be performed in order to achieve such an objective. The updated modal analysis carried out in Section 4.2 enables the modal deformation of the structure to be analyzed and better understood for each of the three modes (see Figure 8). The first mode (i.e. Mode 1L) puts the central body in motion, as well as the upper body. This mode mainly solicites the friction blades, but also the rubber isolators. It is the most complex mode, since the nonlinear contributions of the two nonlinearities are active simultaneously. The second mode (i.e. Mode 2L) is a pumping mode of the upper body, which mostly solicites the rubber isolators. On this mode, it is only expected to see the activation of the elastomer nonlinearity. Then, the third mode (i.e. Mode 3L) puts the envelope structure in motion, which is in contact with the friction blades and can therefore trigger the friction nonlinearity. The elastomers are not much solicited for this mode.

To go further in this prior analysis of the understanding of the role of nonlinearities in the structural response, two sets of complete nonlinear simulations are performed, activating one type of nonlinearity by set of simulations. The objective of this prior analysis is to propose a qualitative study of the contribution of each nonlinearity (the friction blades alone, or the rubber isolators alone), while considering the other type of joints in its linear configuration. Of course, the structure Harmony-Gamma may exhibit complex behaviors where the two nonlinearities have a simultaneous contribution. This type of analysis will be proposed in the section dedicated to the comparisons between experiments and simulations (see Section 7).

Figure 14a presents the simulation results obtained by considering the rubber isolators as linear joints. Only the friction blades are contributing to the nonlinear effects in the simulations. The results are obtained for excitation levels of 162 N, 813 N, 1625 N, 2437 N, 9748 N and 19495 N. First, it is observed that Modes 2L and 3L are independent of the friction joint. However, the first mode (i.e. Mode 1L) is strongly dependent on

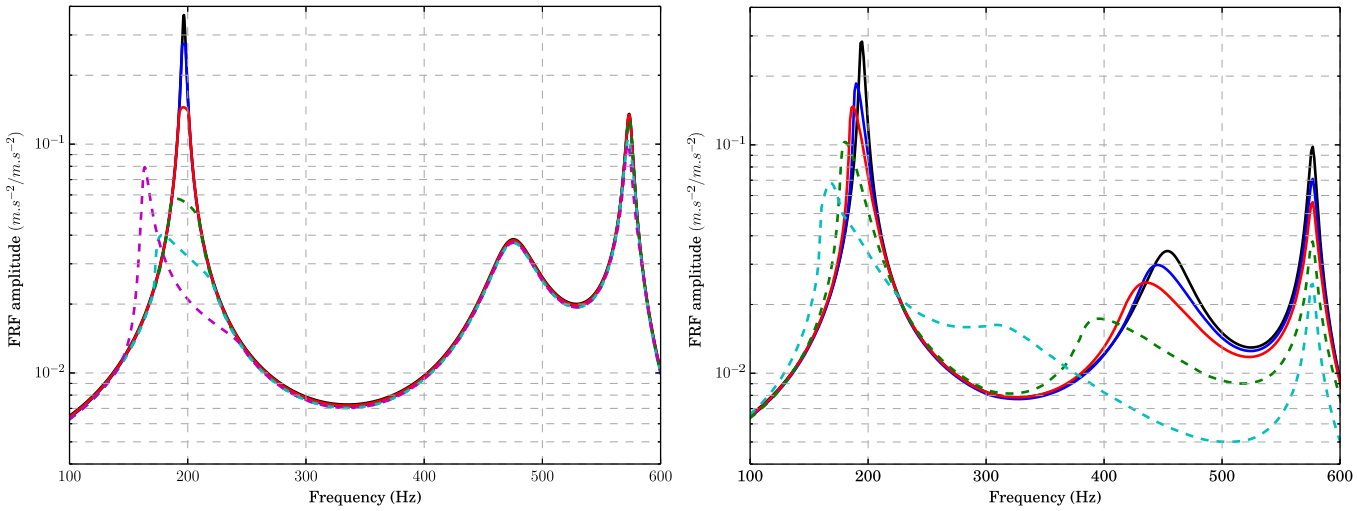

Figure 14: Longitudinal FRFs obtained at the upper body for calculations that only consider (a) the friction nonlinearity for excitation levels of 162 N (black), 813 N (blue), 1625 N (red), 2437 N (green), 9748 N (cyan) and 19495 N (magenta) (b) and only the elastomer nonlinearity for input forces of 162 N (black), 813 N (blue), 1625 N (red), 2437 N (green) and 9748 N (cyan)

the excitation level, which indicates an activation of the nonlinearity at the resonance. With the excitation level increase, the resonance peak is dampened and flattened. The simulations have been performed for excitation levels that could not be performed experimentally, in order to evaluate the behavior of the blades at high excitation levels (see the dotted curves in Figure 14a). It seems that, after a given excitation level, an increase in the latter leads to less dissipation and a softening of the mode. An asymptotic regime is reached when the input force is such that the blades are always sliding on the envelope.

Figure 14b presents the simulation results obtained by considering the blades as linear joints. Only the rubber isolators are contributing to the nonlinear effects in the simulations. Results are obtained for input forces of 162 N (black), 813 N (blue), 1625 N (red), 2437 N (green) and 9748 N (cyan). First, the effect of the rubber isolators is observed on the second resonance mode (i.e. Mode 2L), which was identified in the linear analysis as the pumping mode of the rubber isolators. The third mode (i.e. Mode 2L) is also affected by the nonlinearity of the elastomer, but through a linear interaction: the frequency of the mode remains unchanged, but its resonance peak is lowered because it is farther from the second resonance mode. The third resonance mode is, therefore, indirectly dependent on the nonlinearity of the elastomer. However, the nonlinearity does not affect the frequency or the modal deformation of this mode. Hence, it is concluded that the previous observed experimental phenomena observed around the third resonance mode (i.e. a minor visible phenomenon of hardening effect and jump, see Figure 3) may stem from nonlinearities that have not been taken into account in the present nonlinear model. In the rest of the study, these sources of unknown nonlinearities are neglected, because the hardening effect is negligible compared to the variability of the third mode. Lastly, it is also observed a dependence of the first resonance mode (i.e. mode 1L) on the rubber isolators, with an increase in dissipation and a softening effect. The form of the peak is not flattened and remains approximately the same. Moreover, for a given excitation level, the frequency shift seems more pronounced than in the previous configuration for which only the nonlinearities of the friction blades are considered.

7. Numerical results and comparison with the experiments

The objective of this section is to compare the simulation results with the experiments presented in Section 3.1 for both longitudinal and transverse swept sine experiments on the structure Harmony-Gamma. A specific attention will be paid to better understand the nonlinear experimental behavior of the structure Harmony-Gamma and more specifically the role of the friction and elastomer joints in experiments. In order to achieve such an objective, the analyzes will build on the previous conclusions given in Section 6 that allows to estimate which nonlinearity is affecting what part of the dynamical response of the structure via numerical simulations.

7.1. Longitudinal swept sine tests

7.1.1. Preliminary choice of updating parameters

At the end of the modeling process, the only parameter left to update is the Coulomb threshold $F_{Coulomb,\,z}$. The value of this parameter is chosen at 120 N, in order to obtain the best correlation between experiments and numerical simulation at the first resonance peak, which is the only one dependent on the friction blades. As a comparison, this parameter was identified at a value of 290 N in the previous work of Claeys et al. [6] for the same set of blades. The decrease in the threshold indicates that the friction is easier in the present study.

Considering this unique updating parameter, very good correlations can be obtained which demonstrates the validity of the nonlinear modeling. Nevertheless, a refined choice of updating is proposed in order to further improve the correlations. This additional updating is mainly explained by the variability of each rubber sample and the warm-up of the elastomers according to the levels of excitations. It is also recalled that preliminary experimental identification tests do not use exactly the same elastomer samples as those of the structure Harmony-Gamma, as previously explained in Section 4.4.2). So an updating parameter $alpha_L$ with values between [0.955;0.97] (starting from tests with low levels of excitation to high levels) is added. These values are close to 1, which indicates an initial good quality of the correlation between experiments and simulations without updating, and also the quality of the methodology for the identification of the elastomer behavior presented in Section 4.4.2.

7.1.2. Comparison between experiments and simulations - understanding of the nonlinear phenomena

Figure 15 shows a comparison between the experimental and simulation results for longitudinal excitations, taking into account the two types of nonlinearities. An excellent correlation is observed, at the top of the upper body (see Figure 15a) and the central body (Figure 15c), over the entire frequency bandwidth and for the four tested excitations: 162 N, 813 N, 1625 N and 2437 N.

Comparing Figure 15b with Figure 14a and considering the previous analysis conducted in Section 6, it can be concluded that the frequency shift observed on the first resonance mode (i.e. mode 1L) is mainly due to the rubber isolators. Indeed, for equivalent input excitation levels, it was not observed frequency shift in the previous calculations for which only the friction nonlinearity was taken into account (i.e. the rubber isolators are modeled by linear joints), as indicated in Figure 14a. However, around the first resonance mode, the damping is increased by both he rubber isolators and the friction between the blades and the external envelope. By comparing Figures 14 and 15, it is also obvious that the nonlinear dynamic behavior around the second and third resonance modes (i.e. modes 2L and 3L) is a consequence of rubber isolators.

Figures 15a and 15c display simulation results that have not been tested experimentally due to potential structural damage of the structure for high levels of excitation (see numerical results in cyan and magenta dashed curves). The classical asymptotic behavior and a re-increase in amplitude of the first resonance mode is observed. Considering the previous numerical results in Section 6 on the fact that this asymptotic behavior and this re-increase in amplitude at the first resonance mode are mainly due to the predominant role of the friction joints (see Figure 14a), it can be concluded that this nonlinear phenomenon is mainly characterized by the blades that slip freely on the envelope. Similarly, it can be concluded that the nonlinear behaviors observed for high levels of excitation around the second and third modes are mainly due to the contribution of the elastomers.

In conclusion these comparisons between experiments and simulations for longitudinal swept sine are excellent. This validates the entire nonlinear methodology developed in this work. It also illustrated that a phenomenological nonlinear modeling of the friction and elastomer joints is sufficient to capture the essential of the nonlinear vibrational phenomena. It also allows a good understanding of the roles of both the friction and elastomer joints on the complex nonlinear behavior of the structure Harmony-Gamma.

7.2. Transverse swept sine tests

7.2.1. Preliminary choice of updating parameters

The linear analysis of the transverse case (see Section 4.2) evidenced small discrepancies between the finite modeling analysis of the structure Harmony-Gamma and the experimental results for small excitation levels. More precisely, it was indicated that the modeling defect comes from the mounting of the rubber isolator on the structure Harmony-Gamma. In order to compensate this modeling defect, two updating parameters α_T and α_L have been added for the transverse swept sine tests in the case of the linear updating and validation of the Harmony-Gamma structure (see Section 4.2). This process is now extended to study

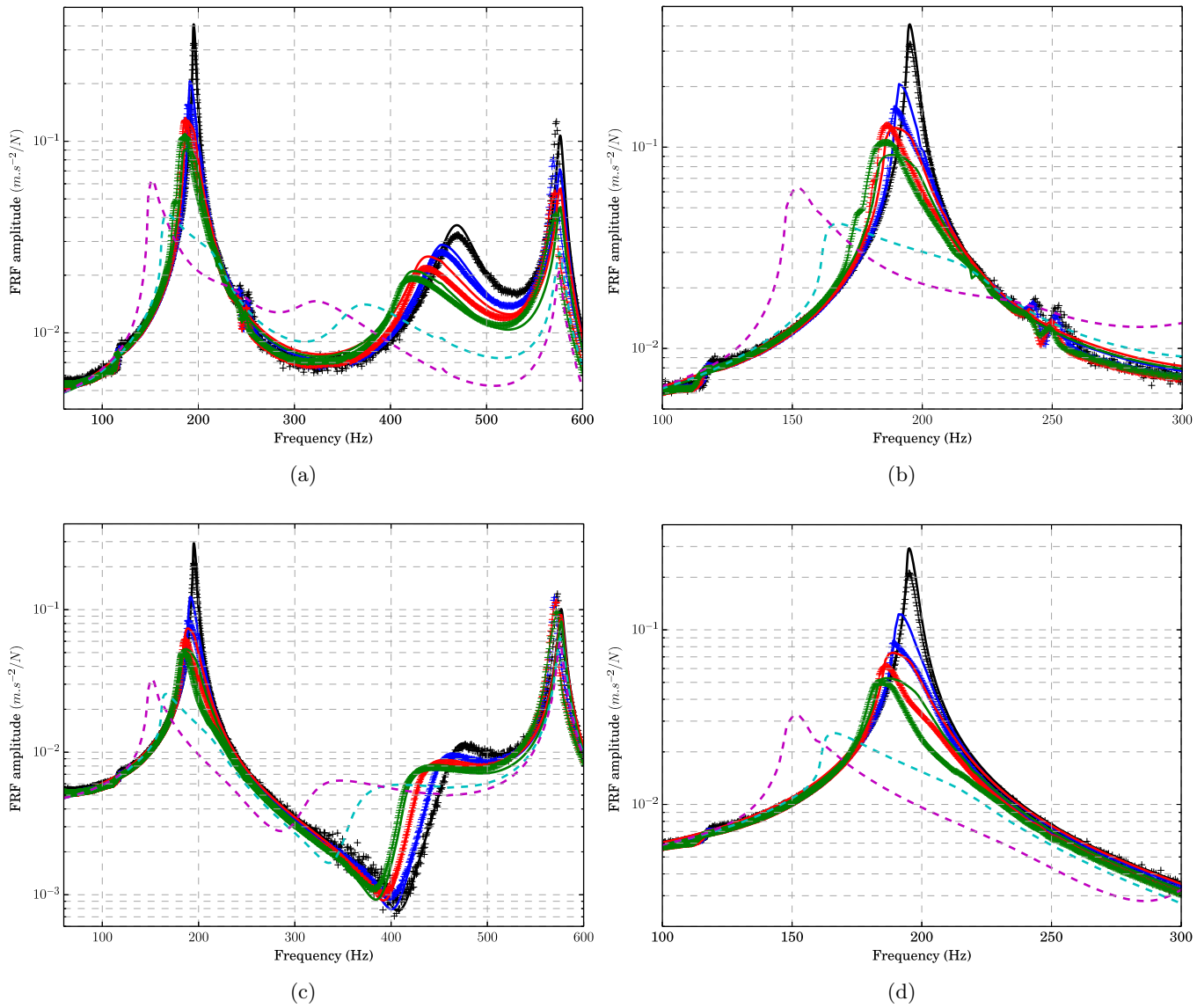

Figure 15: Experimental (crosses) and numerical (plain curves) longitudinal FRF obtained for the accelerometer on the upper body (a,b) and the accelerometer on the central body (c,d) for excitation levels of 162 N (black), 813 N (blue), 1625 N (red), 2437 N (green), 9748 N (cyan) and 19495 N (magenta) (a,c) over the frequency interval of study (b,d) zoom

the general tendencies of the evolution of the transverse frequency response function with respect to the high excitation levels. Table 4 summarizes the evolution of the two parameters α_T and α_L. It can be noted that the decreasing value of α_T for high excitation levels is coherent with the fact that the mounting of the elatomer joint is more flexible in the transverse direction than the mounting of the elastomer joint for the identification process of its nonlinear behavior.

Finally Table 4 give the updating value of the friction parameter $F_{Coulomb,\theta y}$ for the friction modeling previously described in Section 4.4.3. For the interested reader, it can be noted that only $F_{Coulomb,\theta y}$ is updated due to the fact that it allows itself to predict the transverse frequency response of the structure around the first resonance mode, for all levels of excitation.

7.2.2. Comparison between experiments and simulations - understanding of the nonlinear phenomena

Figures 16 present the comparisons between experiments and simulations for the excitation levels 0.5 m s^{-2}, 1 m s^{-2} , 5 m s^{-2} and 10 m s^{-2}. The comparison is achieved for three locations on the structure Harmony-Gamma in order to better assess the global relevance of the comparison in the frequency bandwidth [50;500] Hz.

First, a good correlation for the lowest excitation level is observed. Not only the frequencies and the amplitudes peaks of the four resonance modes (i.e. modes iT for $i = 1, \ldots, 1$) are very close between experiments and simulations, but also the global FRF responses are well reproduced. As a reminder comparison between the numerical and experimental resonance modes and the associated mode shapes of the

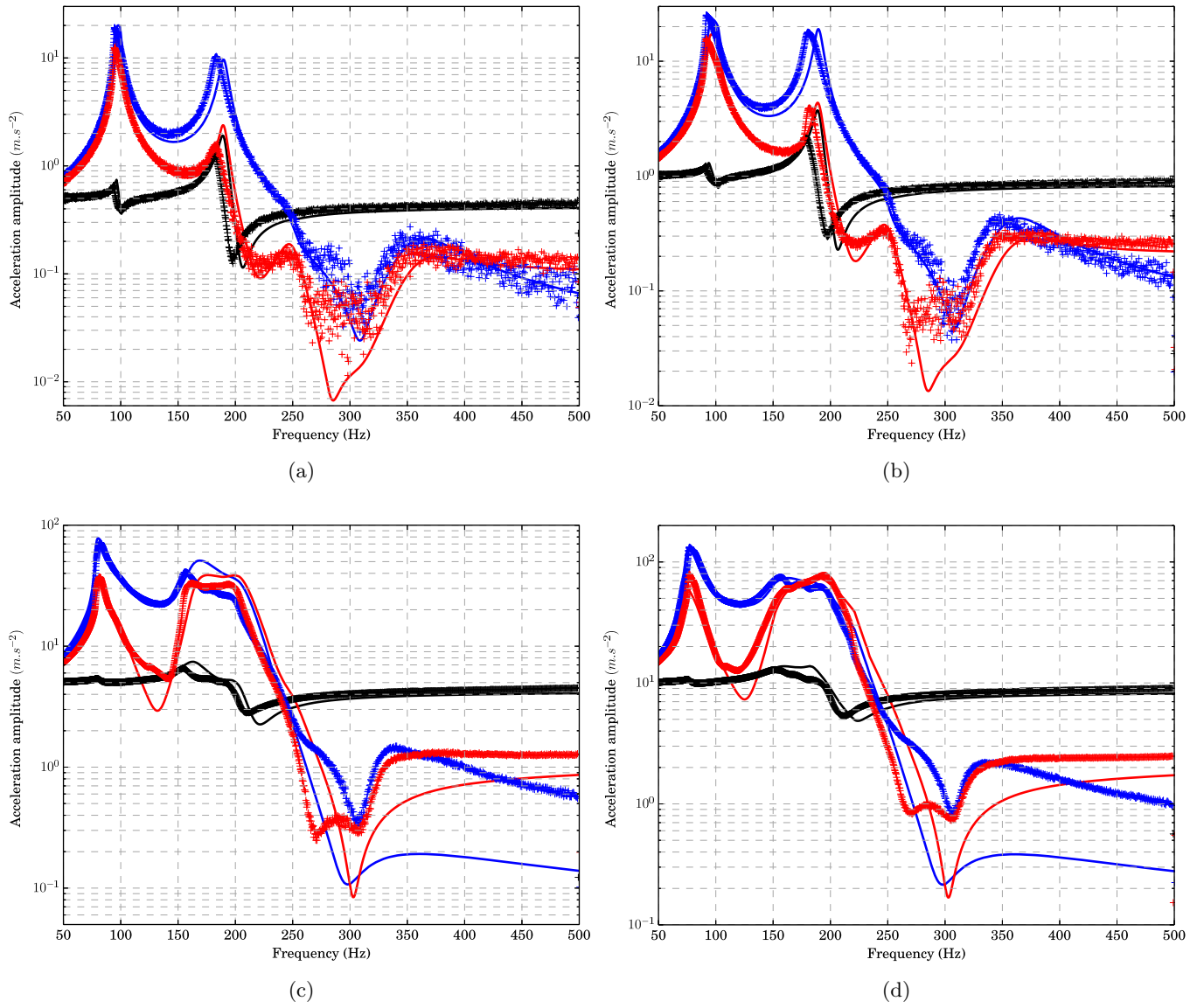

Figure 16: Experimental (crosses) and numerical (plain curves) transverse FRFs for swept sine experiments of (a) 0.5 m s^{-2} (b) 1 m s^{-2} (c) 5 m s^{-2} and (d) 10 m s^{-2} for accelerometers positioned on the upper body (blue), the central body (red) and the base plate (black)

structure Harmony-Gamma are given in Table 3. All these results clearly illustrate the fact that using only two updating parameters (i.e. α_T and α_L) is sufficient to construct efficient modeling of the structure Harmony-Gamma, although the vibratory behavior can be very varied and different in the frequency range of interest. Indeed it is good to recalled that Mode 4T is affected by the transverse stiffness of the rubber isolator (dependence on the updating parameter α_T) while Mode 3T of tilting is affected by both transverse and longitudinal stiffness of the rubber isolator (dependence on the two updating parameters α_T and α_L). Furthermore Mode 1T is affected by the transverse stiffness of the elastomer, while Mode 2T is weakly affected by the longitudinal or transverse stiffness of the elastomer. In Figure 16b, the triggering of the friction around the first resonance mode (i.e. modes 1T) is observed. A shifting with decrease of the resonance frequency that is well represented by the calculations is also visible. For these excitation levels, the friction cannot be responsible for this shift in frequency. So this nonlinear behavior is mainly attributed to the decrease in the transverse stiffness of the rubber isolator.

The response is more complex for high excitation levels. Over the frequency bandwidth [75;100] Hz, an evolution of the resonance frequency of the first resonance mode is observed, together with a saturation of the associated resonance peak, which is typical of friction phenomena. Both nonlinearities of the elastomer isolator and the friction joints act simultaneously around this first resonance mode. As for the longitudinal case, the friction participates mainly in the damping of the response, whereas the rubber isolator is responsible for the frequency shift. Within the frequency bandwidth [150;220] Hz, a saturation of the resonance

	Parameter	0.5 m s^{-2}	1 m s^{-2}	5 m s^{-2}	10 m s^{-2}
α_T	Transverse factor	0.6	0.6	0.15	0.15
α_L	Longitudinal factor	0.82	0.82	0.82	0.82
$F_{Coulomb,\theta y}$	Friction threshold (N m^{-1})	1.25	1.25	1.25	1.25

Table 4: Physical values of the updated parameters

peak with a spreading effect is observed (see more specifically Figures 16c and 16d), whose tendency is well captured by the calculation. As previously discussed in Section 6, this saturation is mainly attributed the nonlinear elastomer joints (see Figure 14b).

Lastly, within the frequency bandwidth [220;500] Hz, a shift of the small resonance peak around 350 Hz is observed when increasing the excitation level. This nonlinear phenomena is mainly due to the fact that the rubber isolator is weakly solicited which leads to the shift of the fourth transverse mode 4T.

8. Conclusion

The major objective of the study is to propose the development of a finite element model for a nonlinear industrial structure with friction or elastomer joints in order to achieve a refined understanding of the nonlinear phenomena and their origin. From the different analysis and results obtained, the following conclusions are reached.

The experimental frequency response functions of the structure Harmony-Gamma present a strong nonlinear behavior. It justifies a modeling that takes into account the nonlinear joints (rubber isolators and friction blades). The nonlinear effects appear as an increase in damping and a softening of the resonance modes. Both effects can be caused by either one of these nonlinearities, and it is not possible to dissociate the role of each nonlinearity through the experimental results only.

To achieve greater insight into the underlying nonlinear phenomena, a complete methodology of modeling and numerical simulation is proposed. This methodology also has the objective of reproducing the nonlinear response of the structure. It is based on the Harmonic Balance Method coupled with a substitution process on the nonlinear DOFs that allows the size of the nonlinear optimization system to be minimized. The first step of this methodology is to model the Harmony-Gamma structure through linear finite-element modeling. The numerical response of this linear model must be perfectly updated for low excitation levels, when the nonlinearities are not active. The modeling and updating strategy for the finite-element modeling has been detailed. The proposed methodology is validated with good correlations between experiments and simulations for longitudinal and transverse excitations in the case of swept sine experiments. This work allows to take into account nonlinear models of joints with different natures, and the study of the structure on several modes of resonance where these nonlinear friction and elastomer joints may have combined effects. The coupling effect of friction and elastomer joints is more specifically observed on the first resonance mode.

Acknowledgment

J.-J. Sinou acknowledges the support of the Institut Universitaire de France.

References

[1] E. Sarrouy, J.-J. Sinou, Non-linear periodic and quasi-periodic vibrations in mechanical systems - on the use of the harmonic balance methods, in: F. Ebrahimi (Ed.), Advances in Vibration Analysis Research, INTECH, Open Access Publisher, 2011, Chapter 21.

[2] C. Pierre, A. Ferri, E. Dowell, Multi-harmonic analysis of dry friction damped systems using an incremental harmonic balance method, Journal of applied mechanics 52 (4) (1985) 958–964.

[3] K. Sanliturk, D. Ewins, Modelling two-dimensional friction contact and its application using harmonic balance method, Journal of sound and vibration 193 (2) (1996) 511–523.

[4] G. Von Groll, D. J. Ewins, The harmonic balance method with arc-length continuation in rotor/stator contact problems, Journal of sound and vibration 241 (2) (2001) 223–233.

[5] V. Jaumouillé, J.-J. Sinou, B. Petitjean, Simulation of payne effect of elastomeric isolators with a harmonic balance method, Shock and Vibration 19 (6) (2012) 1281–1295.

[6] M. Claeys, J. Sinou, J. Lambelin, R. Todeschini, Experiments and numerical simulations of nonlinear vibration responses of an assembly with friction joints–application on a test structure named “harmony”, Mechanical Systems and Signal Processing 70 (2016) 1097–1116.

[7] M. Claeys, J.-J. Sinou, J.-P. Lambelin, R. Todeschini, Modal interactions due to friction in the nonlinear vibration response of the harmony test structure: experiments and simulations, Journal of Sound and Vibration 376 (2016) 131–148.
[8] T. Roncen, J.-J. Sinou, J.-P. Lambelin, Experiments and nonlinear simulations of a rubber isolator subjected to harmonic and random vibrations, Journal of Sound and Vibration 451 (2019) 71 – 83.
[9] M. Kim, V. Belsky, M. Belyi, Substructure generation using automated multilevel substructuring, patent US 2013/0124150A1 and EP 2597578A1 (2013).
[10] W. Hurty, Vibrations of structural systems by component mode synthesis, Journal of the Engineering Mechanics Division 86 (4) (1960) 51–70.
[11] R. Craig, M. Bampton, Coupling of substructure for dynamic analysis, AIAA Journal 1 (2) (1968) 1313–1319.
[12] D. Klerk, D. Rixen, S. Voormeeren, General framework for dynamic substructuring: history, review, and classification of techniques, American Institute of Aeronautics and Astronautics Journal 46 (5) (2008) 1169–1181.
[13] J. Harris, A. Stevenson, On the role of nonlinearity in the dynamic behavior of rubber components, Rubber Chemistry and Technology 59 (5) (1986) 740–764.
[14] M. Sjöberg, L. Kari, Testing of nonlinear interaction effects of sinusoidal and noise excitation on rubber isolator stiffness, Polymer Testing 22 (3) (2003) 343 – 351.
[15] R. Lewandowski, B. Chorazyczewski, Identification of the parameters of the kelvin–voigt and the maxwell fractional models, used to modeling of viscoelastic dampers, Computers and Structures 88 (1) (2010) 1 – 17.
[16] M. M. Sjöberg, L. Kari, Non-linear behavior of a rubber isolator system using fractional derivatives, Vehicle System Dynamics 37 (3) (2002) 217–236.
[17] M. Berg, A non-linear rubber spring model for rail vehicle dynamics analysis, Vehicle System Dynamics 30 (3-4) (1998) 197–212.
[18] D. Jalocha, A. Constantinescu, R. Neviere, Prestrain-dependent viscosity of a highly filled elastomer: experiments and modeling, Mechanics of Time-Dependent Materials 19 (3) (2015) 243–262.
[19] N. Gil-Negrete, J. Vinolas, L. Kari, A simplified methodology to predict the dynamic stiffness of carbon-black filled rubber isolators using a finite element code, Journal of Sound and vibration 296 (4-5) (2006) 757–776.
[20] C. Xueqian, S. Zhanpeng, H. Qinshu, D. Qiang, L. Xin'en, Influence of uncertainty and excitation amplitude on the vibration characteristics of rubber isolators, Journal of Sound and Vibration 377 (2016) 216–225.
[21] D.-w. Sun, Z.-g. Chen, G.-y. Zhang, P. Eberhard, Modeling and parameter identification of amplitude-and frequency-dependent rubber isolator, Journal of Central South University of Technology 18 (3) (2011) 672.
[22] P. Dahl, Solid friction damping of mechanical vibrations, AIAA Journal of Guidance, Control and Dynamics 14 (1976) 1675–1682.
[23] W. Iwan, A distributed-element model for hysteresis and its steady-state dynamic response, Journal of Applied Mechanics 33 (1966) 893–900.
[24] L. Gaul, J. Lenz, Nonlinear dynamics of structures assembled by bolted joints, Acta Mechanica 125 (1-4) (1997) 169–181.
[25] L. Gaul, R. Nitsche, The role of friction in mechanical joints, Applied Mechanics Reviews 54 (2) (2001) 93–106.
[26] D. Segalman, A four-parameter iwan model for lap-type joints, Journal of Applied Mechanics 72 (5) (2005) 752–760.
[27] M. Rajaei, H. Ahmadian, Development of generalized iwan model to simulate frictional contacts with variable normal loads, Applied Mathematical Modelling 38 (15) (2014) 4006–4018.
[28] D. Roettgen, M. Allen, Nonlinear characterization of a bolted, industrial structure using a modal framework, Mechanical Systems and Signal Processing 84 (2017) 152 – 170, recent advances in nonlinear system identification.
[29] C. Schwingshackl, E. Petrov, D. Ewins, Measured and estimated friction interface parameters in a nonlinear dynamic analysis, Mechanical Systems and Signal Processing 28 (2012) 574 – 584.
[30] R. Lacayo, L. Pesaresi, J. Groß, D. Fochler, J. Armand, L. Salles, C. Schwingshackl, M. Allen, M. Brake, Nonlinear modeling of structures with bolted joints: A comparison of two approaches based on a time-domain and frequency-domain solver, Mechanical Systems and Signal Processing 114 (2019) 413 – 438.
[31] M. Brake, The Mechanics of Jointed Structures: Recent Research and Open Challenges for Developing Predictive Models for Structural Dynamics - Chapter 14, Springer, 2018.
[32] J. Guillen, C. Pierre, An efficient, hybrid, frequency-time domain method for the dynamics of large-scale dry-friction damped structural systems., in: IUTAM Symposium on Unilateral Multibody Contacts, Springer, 1999, pp. 169–178.
[33] E. Hahn, P. Chen, Harmonic balance analysis of general squeeze film damped multidegree-of-freedom rotor bearing systems, Journal of Tribology 116 (1994) 499–507.
[34] J.-J. Sinou, Non-linear dynamics and contacts of an unbalanced flexible rotor supported on ball bearings, Mechanism and Machine Theory 44 (2009) 1713–1732.
[35] T. Cameron, J. Griffin, An alternating frequency time domain method for calculating the steady state response of nonlinear dynamic systems, ASME Journal of Applied Mechanics 56 (1989) 149–154.